The Abdus Salam International Centre for Theoretical Physics

United Nations Educational, Scientific and Cultural Organization

IAEA International Atomic Energy Agency

2048-1

From Core to Crust: Towards an Integrated Vision of Earth's Interior

20 - 24 July 2009

Structure and Non-Linear Dynamics of the Earth

G. Panza
Universita di Trieste, Italy

Structure and Non-Linear Dynamics of the Earth

by

Giuliano F. Panza

From Core to Crust: Towards an Integrated Vision of Earth’s Interior

ICTP - 20/24 July 2009

SAND - Structure and Non-Linear Dynamics of the Earth

The first line of reserach of the ICTP SAND activity is on non-linear dynamics with application to earthquake prediction and to the estimation of seismic risk including: non-linear dynamics of lithosphere blocks and development and testing of algorithms for earthquake prediction. The second line is structure of the earth with application to seismic risk mitigation including: physical instability of megacities (PIOM), deterministic seismic hazard assessment, 3D mapping.

Plates move

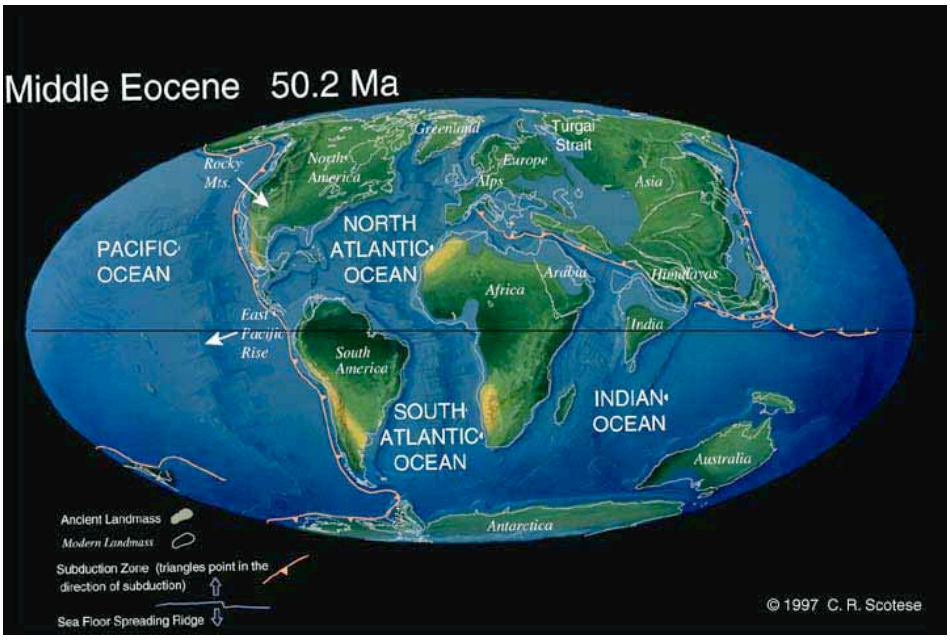
Middle Eocene 50.2 Ma
Greenland
Turgai Strait
Rocky Mts.
North America
Europe
Alps
Asia
NORTH ATLANTIC OCEAN
PACIFIC OCEAN
Arabia
Himalayas
Africa
East Pacific Rise
India
South America
SOUTH ATLANTIC OCEAN
INDIAN OCEAN
Australia
Antarctica
Ancient Landmass
Modern Landmass
Subduction Zone (triangles point in the direction of subduction)
Sea Floor Spreading Ridge
© 1997 C. R. Scotese

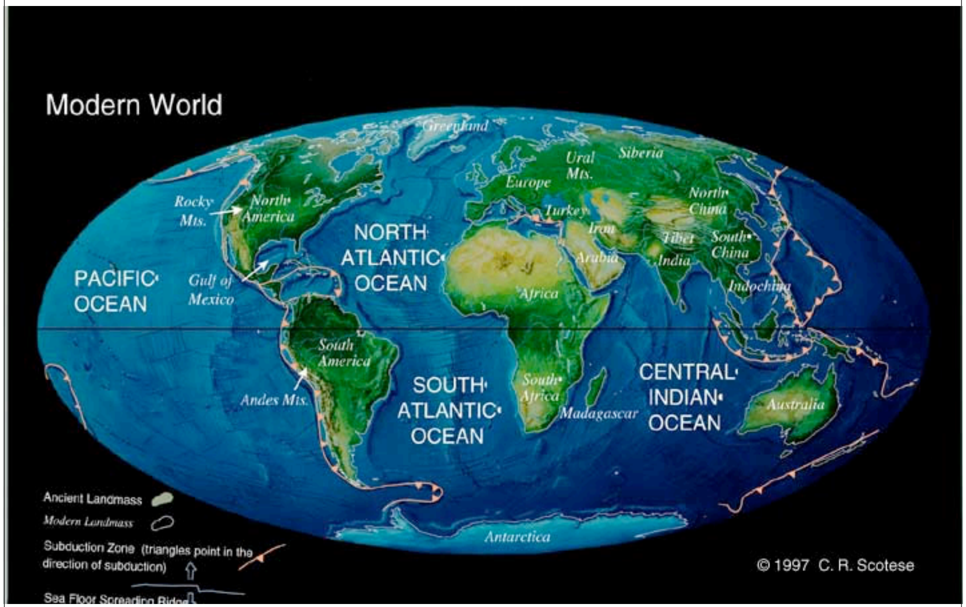

Modern World
Greenland
Siberia
Ural Mts.
Europe
North China
Turkey
Iran
Tibet
South China
Arabia
India
Indochina
Rocky Mts.
North America
NORTH ATLANTIC OCEAN
PACIFIC OCEAN
Gulf of Mexico
Africa
South America
Andes Mts.
SOUTH ATLANTIC OCEAN
South Africa
Madagascar
CENTRAL INDIAN OCEAN
Australia
Antarctica
Ancient Landmass
Modern Landmass
Subduction Zone (triangles point in the direction of subduction)
© 1997 C. R. Scotese

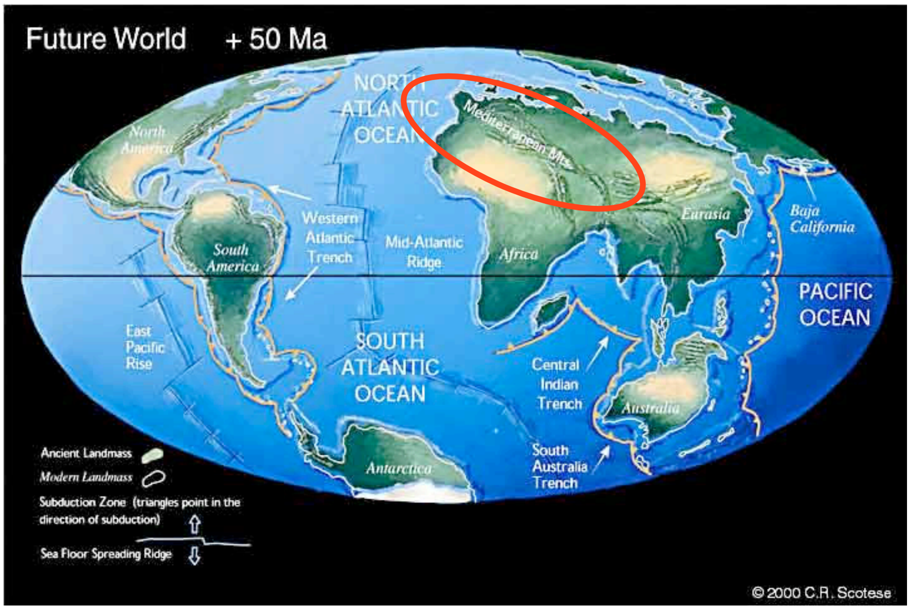

Future World + 50 Ma
NORTH ATLANTIC OCEAN
Mediterranean Mts.
North America
Eurasia
Baja California
Western Atlantic Trench
Mid-Atlantic Ridge
Africa
South America
PACIFIC OCEAN
East Pacific Rise
SOUTH ATLANTIC OCEAN
Central Indian Trench
Australia
South Australia Trench
Antarctica
Ancient Landmass
Modern Landmass
Subduction Zone (triangles point in the direction of subduction)
Sea Floor Spreading Ridge
© 2000 C.R. Scotese

However, there are still fundamental questions to be answered: are plates dragged horizontally by mantle convection? Are they dragged and sheared at the base by a faster moving mantle? Are they rather pulled by slab pull forces? Could they be driven by Earth's rotation and tidal drag? If ridges and subduction zones trigger convection, but are nevertheless still passive features, what moves plates?

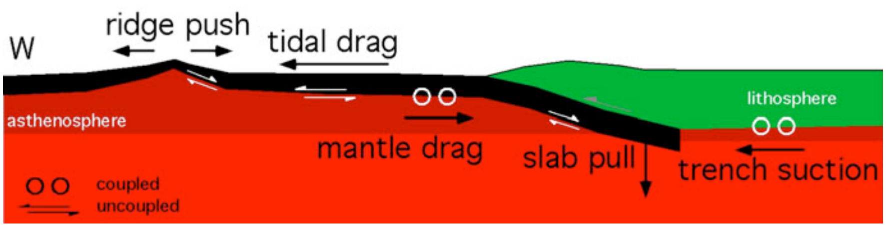

Main forces acting on the lithosphere. Mantle drag and trench suction need high coupling (higher viscosity) between lithosphere and asthenosphere to be more effective. Ridge push, slab pull and tidal drag should rather need low coupling (lower viscosity) to be efficient. Since the lithosphere is decoupled with respect to the asthenosphere, possibly more than one force is actively forcing plate motions. Circles indicate coupled forces, white half arrows show the uncoupled forces (after Doglioni et al., 2007).

The subduction of continental lithosphere is a paradox accordingly with the most popular interpretations of global tectonics, which state that subduction and plate’s tectonics are, as a rule, controlled by the weight of the slab. It is well known that continental lithosphere (not only the crust, but also the lithospheric mantle) is lighter than the underlying mantle, nevertheless the subduction of continental lithosphere, proposed by Ampferer in 1906 and proven by Panza & Muller in 1978, is now widely accepted.

Mountain ranges sitting on continental lithosphere subduction form both:

(a)when the subduction hinge approaches the overriding plate (Alps, Dinarides, Zagros, Himalaya) - type-A subduction - and

(b)when the subduction hinge departs from it (Apennines, Carpathian, Banda) - type-B subduction.

These two modes of continental lithosphere subduction have significantly different characters:

(1) in type-A subduction the mountain ranges are quite high (on average>1500m), show a complete metamorphic cycle and extended basement outcrops, double vergence, two foredeeps subsiding at a rate<0.3mm/y, detachment planes involving the entire crust and the lid and relatively low effusive magmatism;

(2) in type-B subduction the elevation is low, the vergence is single, the well pronounced foredeep subsides at a rate>1mm/y, detachment planes involve mostly the uppermost (1-12 km) subducting crust. At global scale, type-B subductions are west directed, and are overridden by a back-arc basin.

In the central Mediterranean area the examples are Apennines (B), Alps (A),

Dinarides (A), Carpathian(B), where the subduction of continental material is a well-documented phenomenon by the geochemical properties of magmatism (Peccerillo, 2005).

Still the engine of plate tectonics in not too well known. In fact, convection alone seem not able to supply enough energy. This deficit is made even more severe by the the results of Laio, Chiarotti, Scandolo, Bernard and Erio Tosatti who reproduced in the computer the same conditions at the Earth core by solving the fundamental equations governing the dinamics of Iron atoms and estimated a temperature for the Earth core of about 5400 °C, i.e. at lease 1000°C less than what previously estimated. Some relevant amount of energy may be supplied by the deceleration of the Earth rotation due to the Moon (Sun) tidal effect.

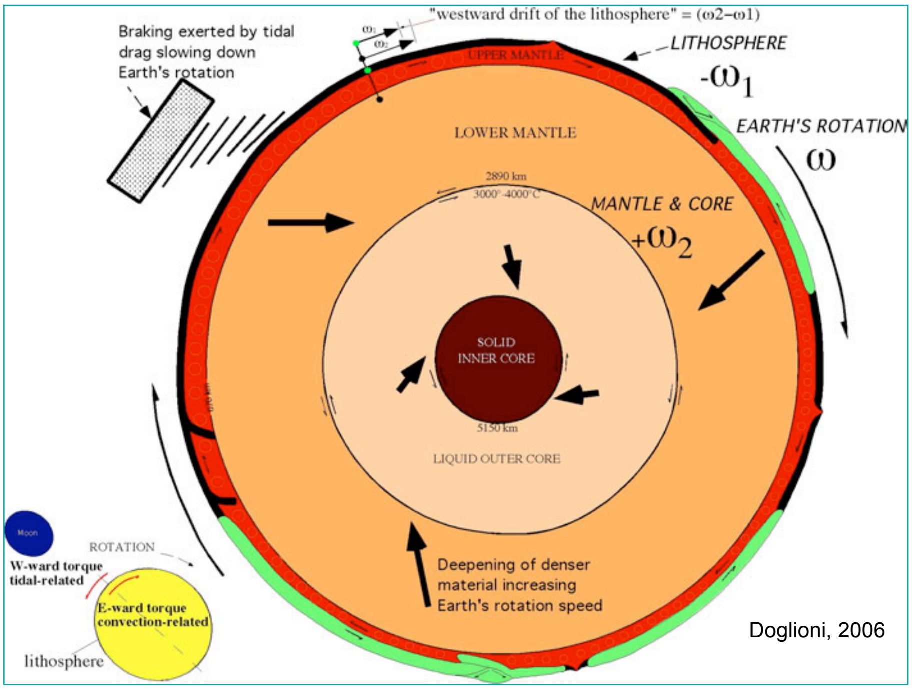

WHAT CAN WE MEASURE?

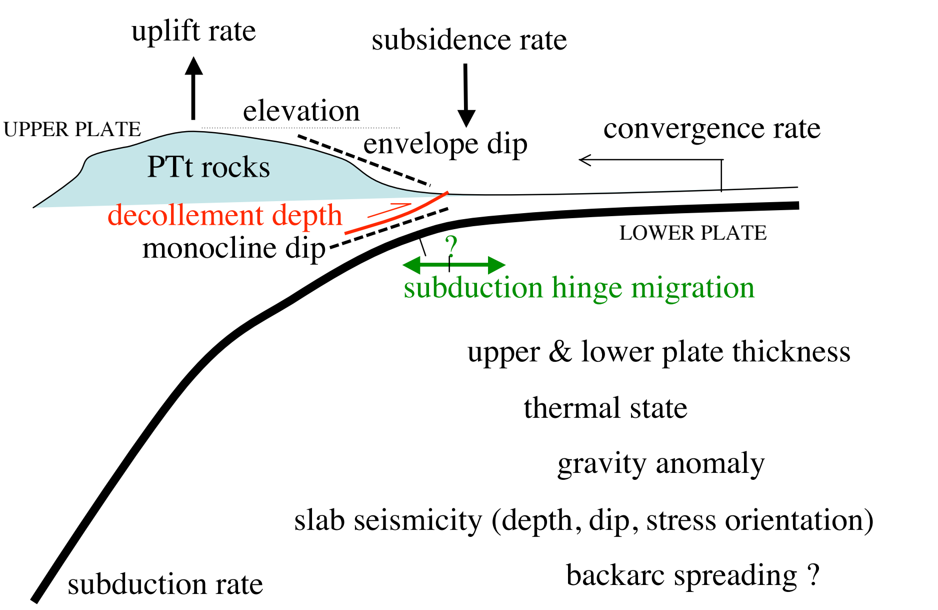

Mountain ranges

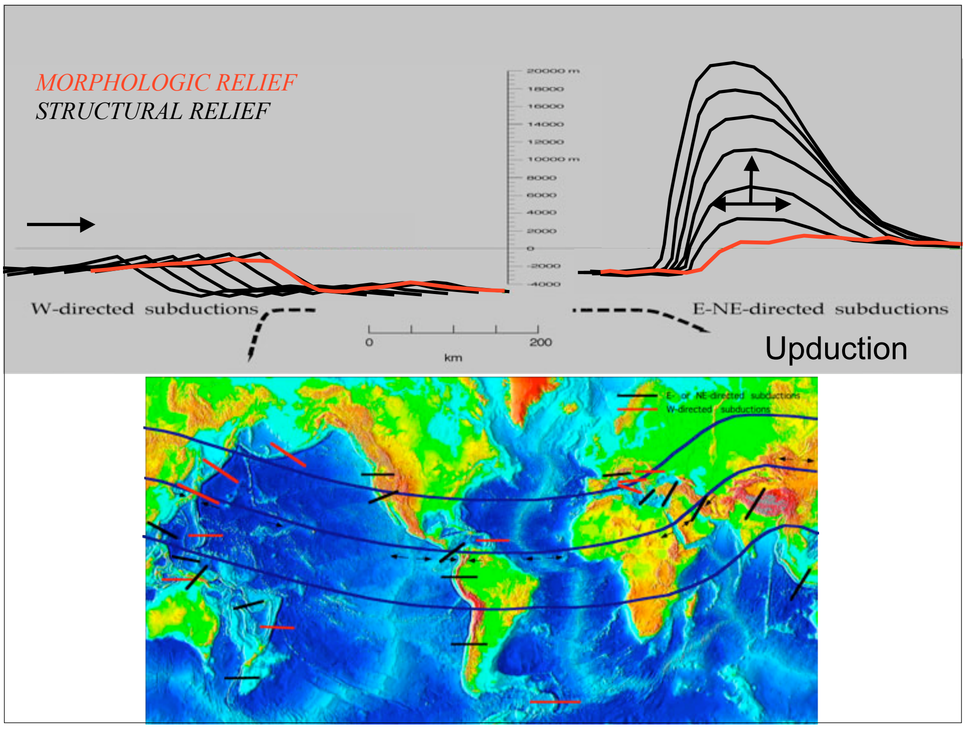
MORPHOLOGIC RELIEF
STRUCTURAL RELIEF
W-directed subductions
E-NE-directed subductions
Upduction
km
0
200

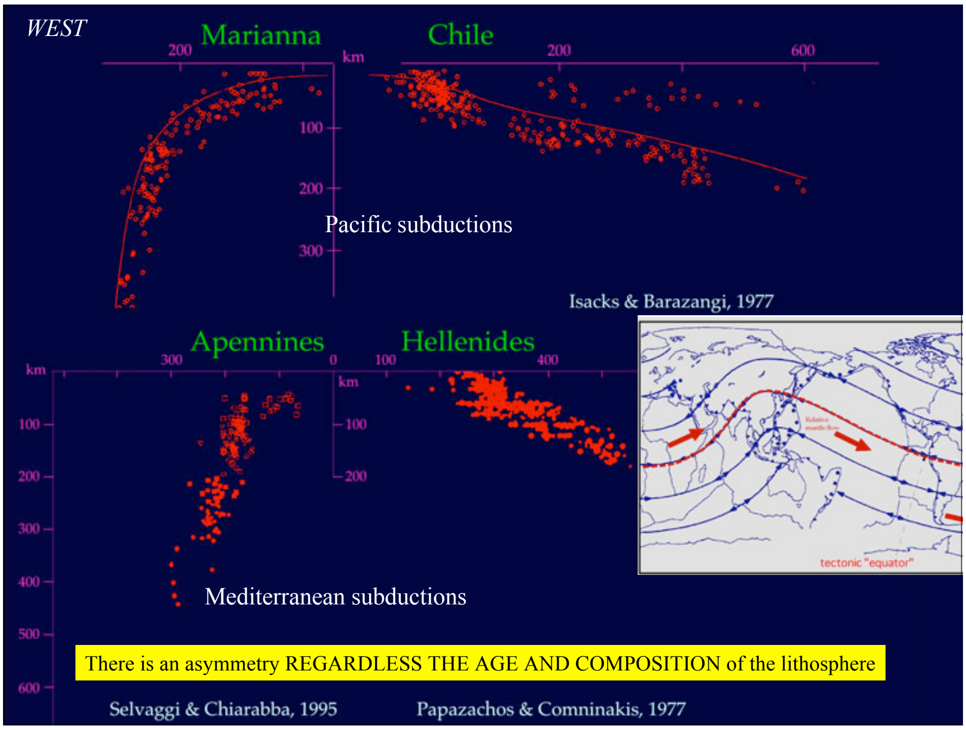
WEST
Marianna
Chile
Pacific subductions
Isacks & Barazangi, 1977
Apennines
Hellenides
Mediterranean subductions
tectonic "equator"
There is an asymmetry REGARDLESS THE AGE AND COMPOSITION of the lithosphere
Selvaggi & Chiarabba, 1995
Papazachos & Comninakis, 1977

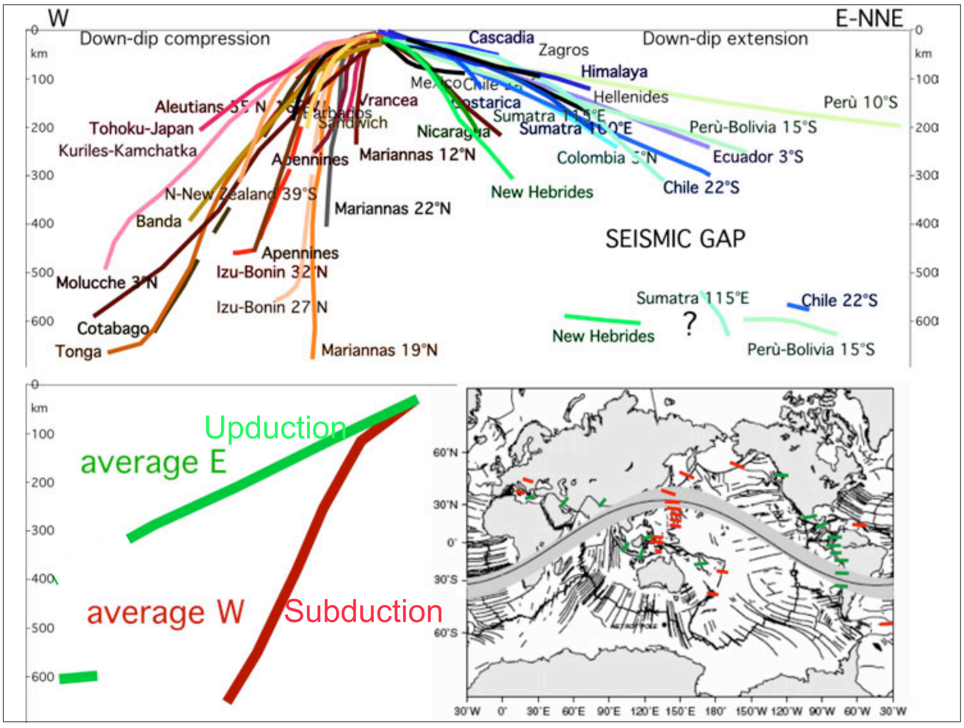

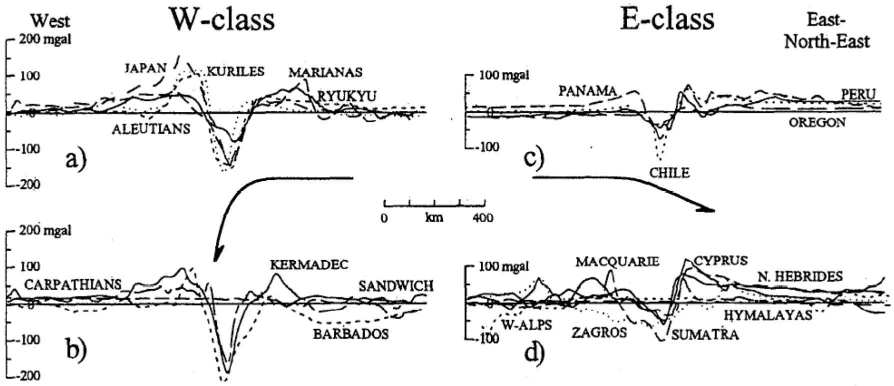

Free-air gravimetric profiles grouped into W-class and E-class

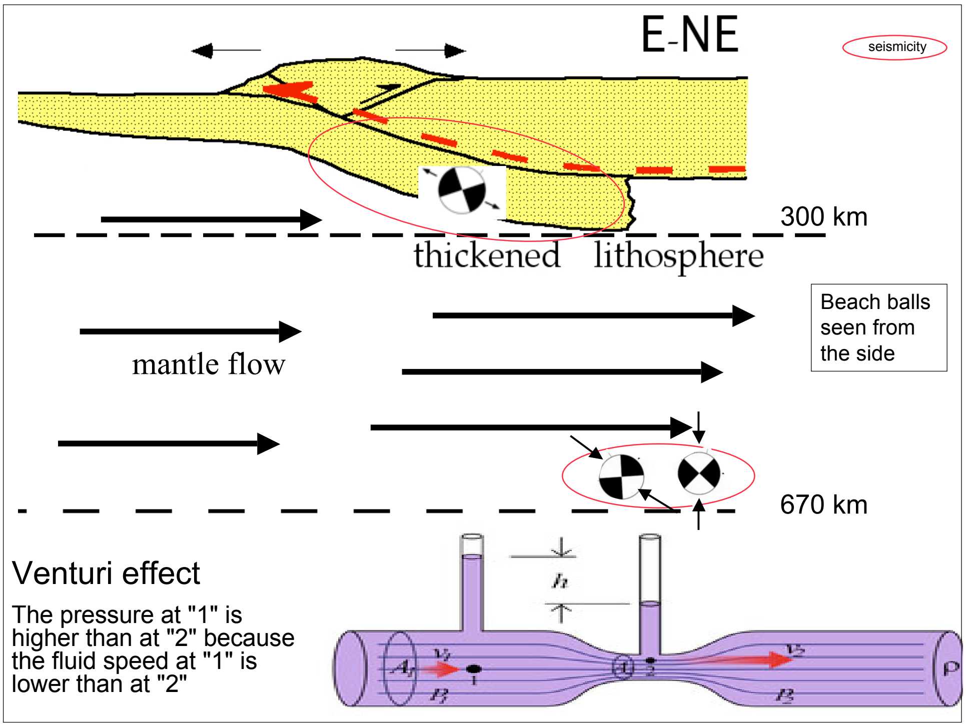

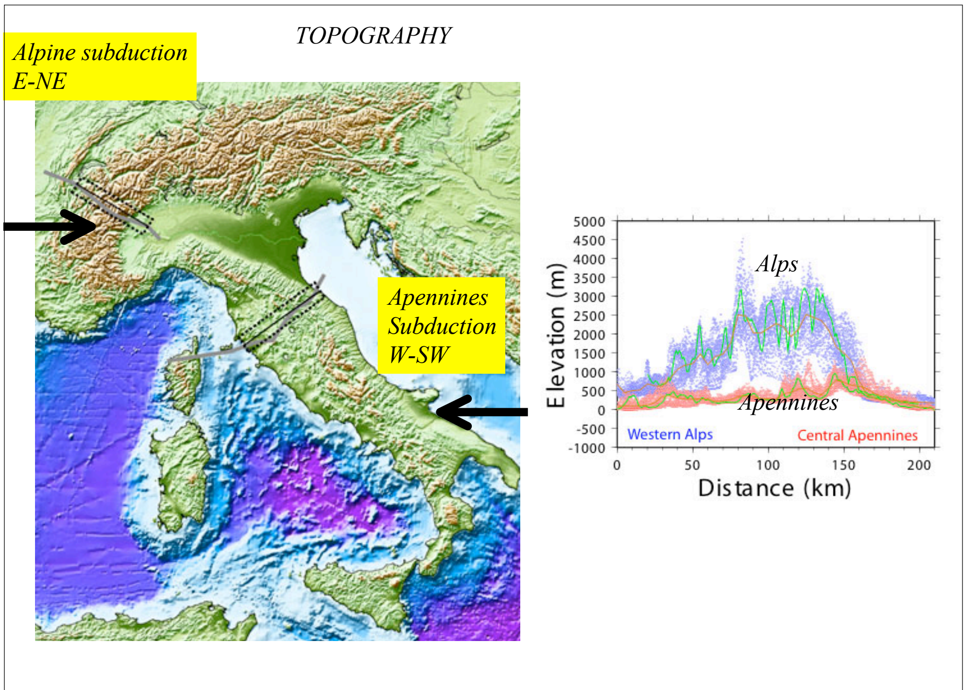

Carminati et al., 2004 SGI

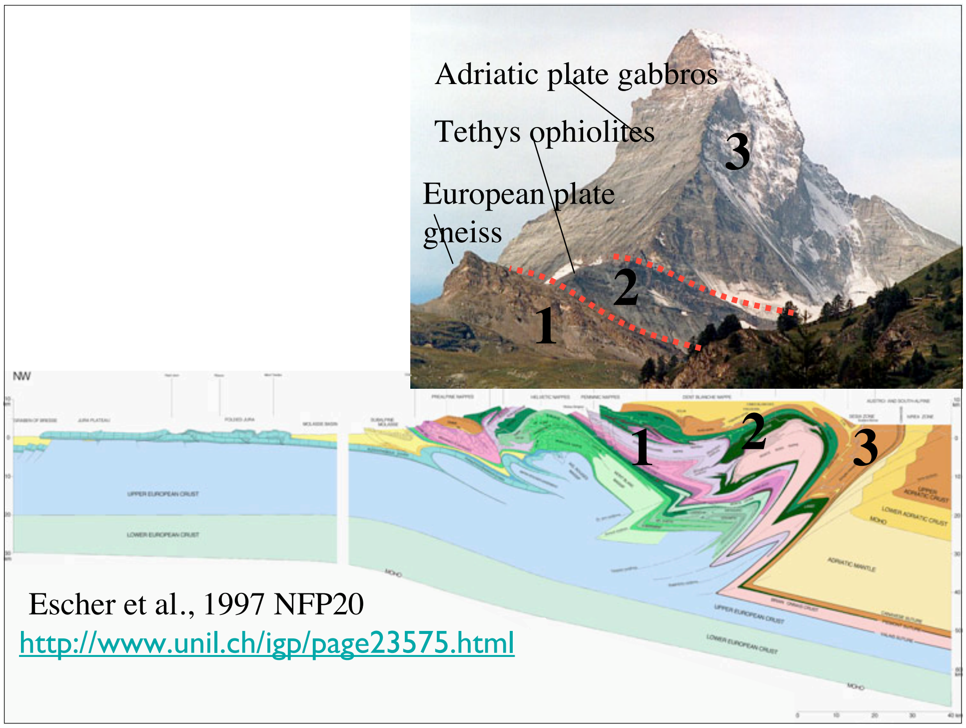
Adriatic plate gabbros
Tethys ophiolites
European plate
gneiss
3
2
1
NW
1
2
3
Escher et al., 1997 NFP20
http://www.unil.ch/igp/page23575.html

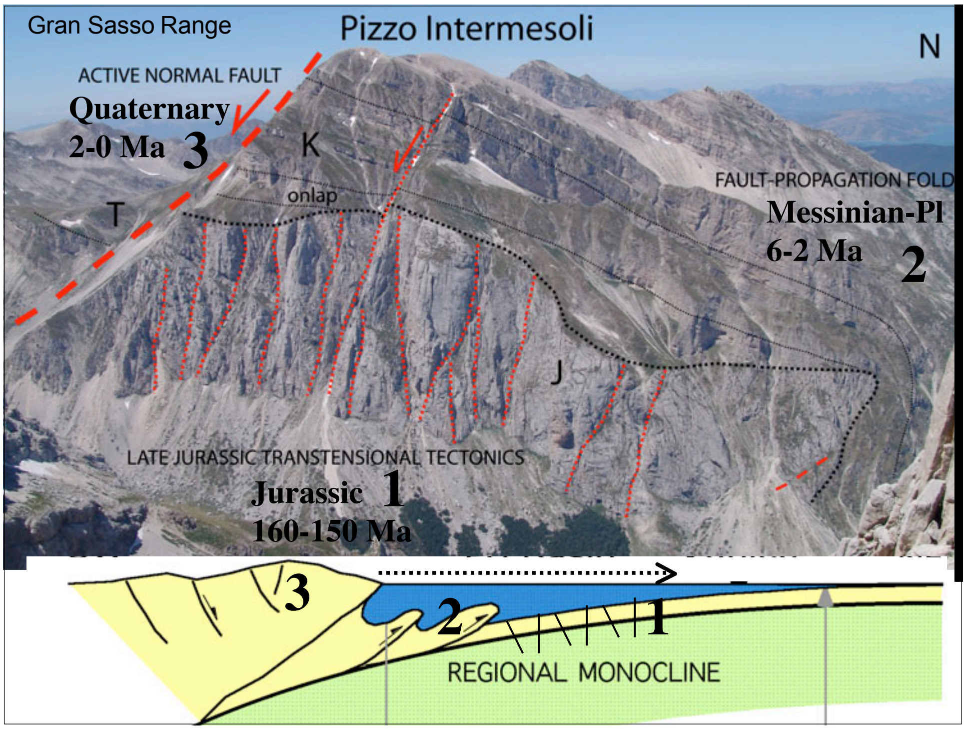
Gran Sasso Range
Pizzo Intermesoli
N
ACTIVE NORMAL FAULT
Quaternary
2-0 Ma 3
K
T
onlap
FAULT-PROPAGATION FOLD
Messinian-Pl
6-2 Ma 2
J
LATE JURASSIC TRANSTENSIONAL TECTONICS
Jurassic 1
160-150 Ma
3
2
1
REGIONAL MONOCLINE

Cross-sections along the Alps,

Panza et al., Le Scienze, 1980

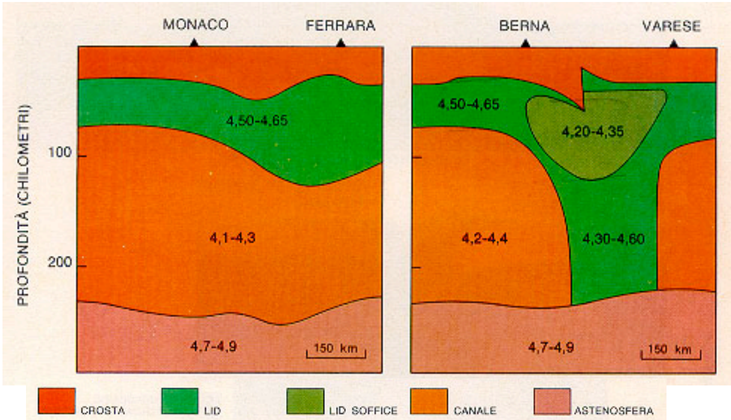

Sezioni verticali attraverso le Alpi orientali *(a)*, centro-occidentali *(b)* e attraverso gli Appennini *(c)*. Nella sezione *a* il massimo ispessimento del lid è spostato verso sud rispetto alle radici crostali. (La radice profonda è interpretata come un raddoppiamento litosferico conseguente la collisione Europa-Africa.) È evidente la assoluta inadeguatezza del concetto di radici crostali per le catene montuose, poiché le variazioni laterali in corrispondenza di zone orogeniche si estendono a profondità superiori ai 200 chilometri. Anche il concetto di isostasia crostale deve essere rivisto perché sia possibile assegnare alle anomalie isostatiche un realistico significato geodinamico. Nella sezione *b*, in corrispondenza della zona di massima deformazione, vi è una porzione di mantello soffice che sovrasta una radice litosferica caratterizzata da alti valori di rigidità, che interrompe il canale a bassa velocità. Anche l'Appennino è caratterizzato (sezione *c*) da una porzione di mantello soffice sovrastante una radice litosferica con rigidità elevata. Notevole è la differenza di spessore tra il lid dell'Adriatico e quello del Tirreno. Tutte e tre le sezioni presentano forti variazioni laterali nelle proprietà elastiche del sistema litosfera--astenosfera (la cui entità è stimata in base agli intervalli di variabilità delle velocità delle onde di taglio riportate nelle sezioni) che interessano anche la base del canale-astenosfera.

Mueller & Panza, 1986

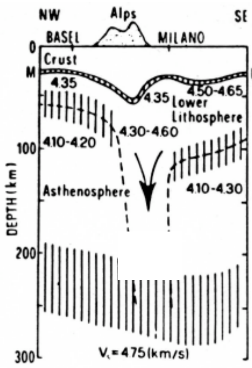

Fig. 2. Crust-mantle cross section derived from the simultaneous inversion of available surface waves dispersion data (after Panza and Mueller, 1979). Hatched areas indicate the range of uncertainty of the bottom of the crust (M), of the lithosphere and of the upper asthenosphere. In the collision process the lower lithosphere has penetrated into the asthenosphere thus forming a nearly vertical zone of "subfluence" ("Verschluckung").

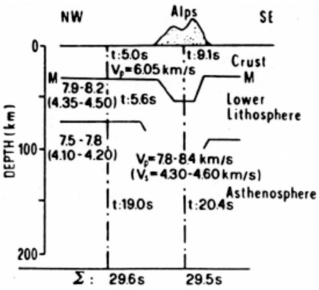

Fig. 3. Schematic crust-mantle cross section through the Central Alps along the Swiss Geotraverse (compare with Fig. 2, after Panza and Mueller, 1979). The one-way travel times of P-waves propagating vertically upwards from the bottom of the upper asthenosphere to the surface corroborate the hypothesis that the time delay caused by the low-velocity crustal root must be compensated by the under-lying high-velocity "litho-spheric root" which is sinking into the asthenosphere (after Baer, 1980). In the model a ratio V_p/V_s of 1.82 has been assumed.

Mueller & Panza, 1986

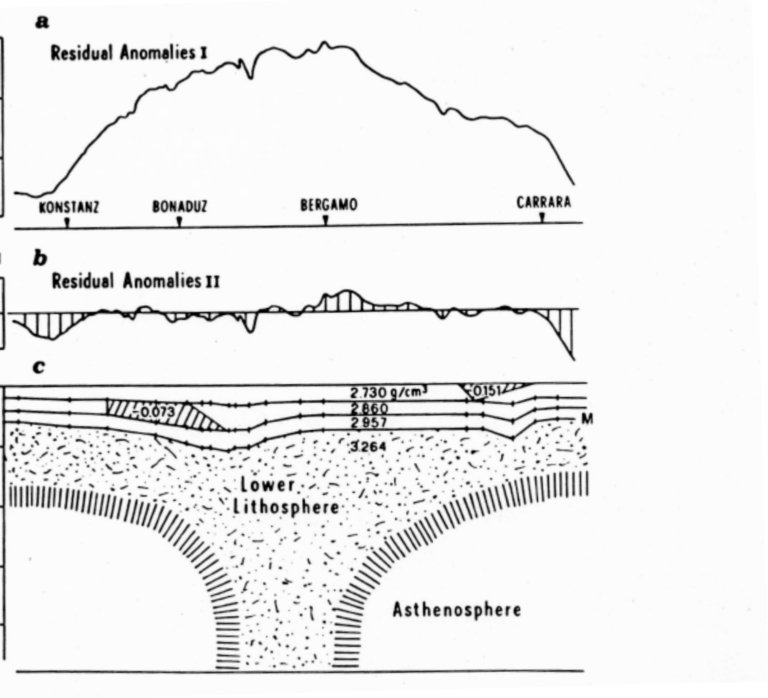

Reprinted from Nature, Vol. 296, No. 5854, pp.238-239, 18 March 1982

64

Delineation of the North Central Italian upper mantle anomaly

G. F. Panza*, St. Mueller†, G. Calcagnile‡ & L. Knopoff§

* Istituto di Geodesia e Geofisica, Università di Trieste, Trieste, Italy
† ETH-Geophysics, Zurich, Switzerland
‡ Istituto di Geodesia e Geofisica, Università di Bari, Bari, Italy
§ Institute of Geophysics and Planetary Physics, University of California, Los Angeles 90024, USA

The Italian peninsula is the focus of intense deformational tectonic activity. It is underlain by mantle material whose inferred, relatively anomalous properties[1,2] are not inconsistent with the seismic, volcanic and thermal activity that is manifested in this region. The most effective geophysical tool for mapping the structure of the uppermost 200–300 km of the Earth is the observation and analysis of seismic surface-wave dispersion on a regional scale. Here we synthesize the interpretations of Rayleigh wave dispersion measurements made by several authors, each for different parts of North Central Italy[3-8], to delineate the lateral extent of the upper mantle anomaly in this region.

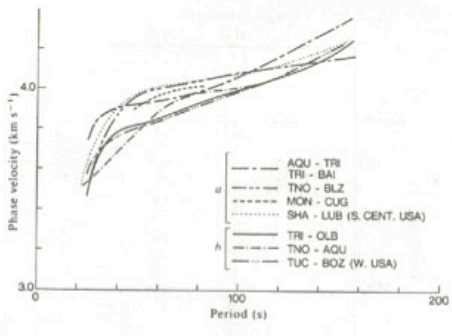

Fig. 2 Phase velocities used to delineate the North Central Italian anomaly and comparison with dispersion relations for western and South-Central USA. The r.m.s. errors for each curve are ~±0.03 km s^{-1} in the period range 40–60 s and are larger at the extremes of the period range[3,5-9]. Curves in group *a* are for regions without tectonic involvement and in group *b* for regions with tectonic involvement.

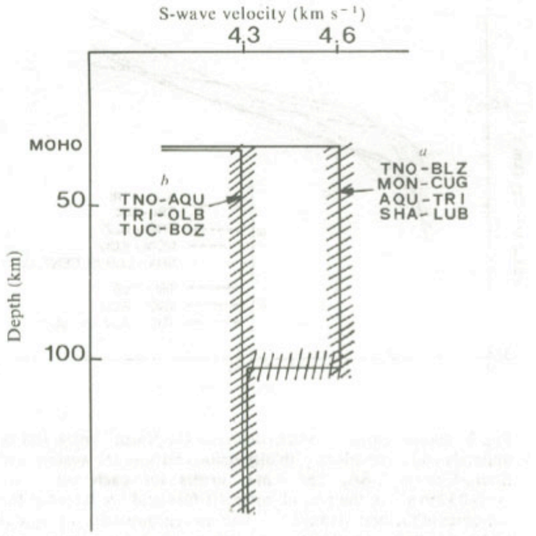

Fig. 3 Schematic shear wave velocity–depth distributions in the upper mantle for regions without *a* and with *b* major tectonic involvement today. The shading represents schematically the range of models satisfying each group of dispersion data.

We concluded that the anomalous low phase velocity region of nortehrn Italy lies to the east of the path MON-CUG, to the west of AQU-TRI, and south of the Alps.

Cross-sections along the Apennines

Panza et al., Le Scienze, 1980

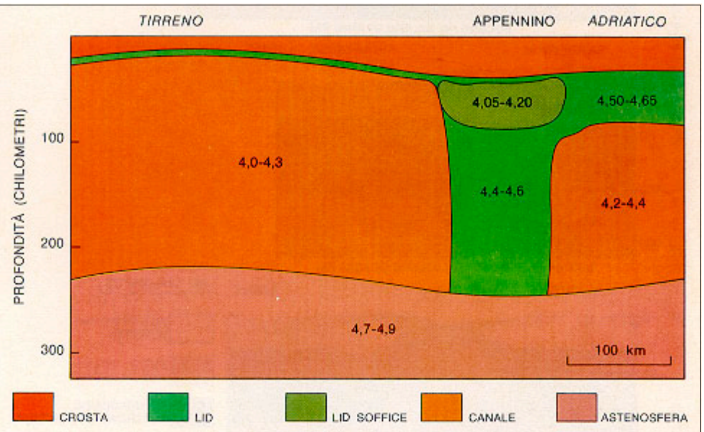

Sezioni verticali attraverso le Alpi orientali *(a)*, centro-occidentali *(b)* e attraverso gli Appennini *(c)*. Nella sezione *a* il massimo ispessimento del lid è spostato verso sud rispetto alle radici crostali. (La radice profonda è interpretata come un raddoppiamento litosferico conseguente la collisione Europa-Africa.) È evidente la assoluta inadeguatezza del concetto di radici crostali per le catene montuose, poiché le variazioni laterali in corrispondenza di zone orogeniche si estendono a profondità superiori ai 200 chilometri. Anche il concetto di isostasia crostale deve essere rivisto perché sia possibile assegnare alle anomalie isostatiche un realistico significato geodinamico. Nella sezione *b*, in corrispondenza della zona di massima deformazione, vi è una porzione di mantello soffice che sovrasta una radice litosferica caratterizzata da alti valori di rigidità, che interrompe il canale a bassa velocità. Anche l'Appennino è caratterizzato (sezione *c*) da una porzione di mantello soffice sovrastante una radice litosferica con rigidità elevata. Notevole è la differenza di spessore tra il lid dell'Adriatico e quello del Tirreno. Tutte e tre le sezioni presentano forti variazioni laterali nelle proprietà elastiche del sistema litosfera-astenosfera (la cui entità è stimata in base agli intervalli di variabilità delle velocità delle onde di taglio riportate nelle sezioni) che interessano anche la base del canale-astenosfera.

V_s versus depth and hypocentres of the sub-crustal earthquakes (vertical bars indicate depth error) in the period 1965-1998 within a stripe 150 km wide along the study profile (red line in the inset). The bold black segment indicates the Moho depth.

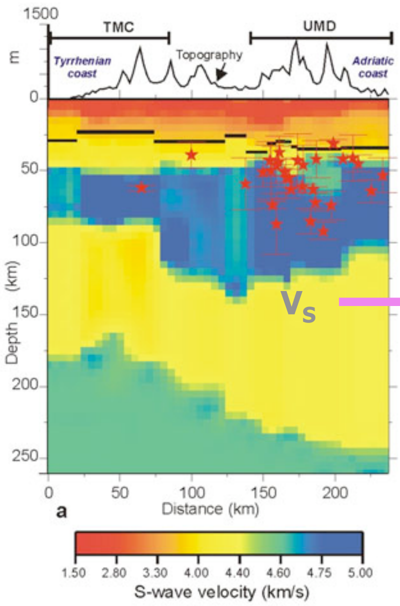

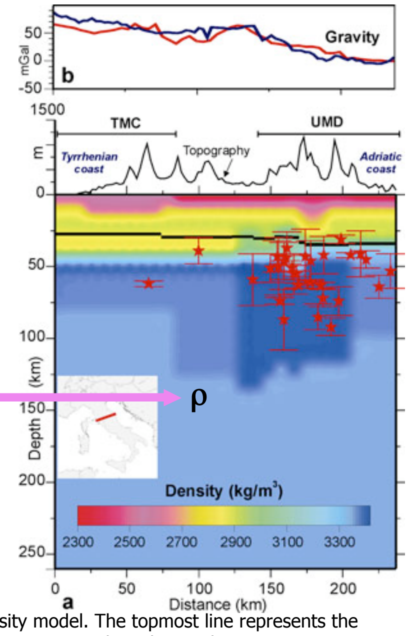

Density model. The topmost line represents the surface topography. Observed Bouguer gravity anomaly (blue) vs. gravity (red) predicted from our density model.

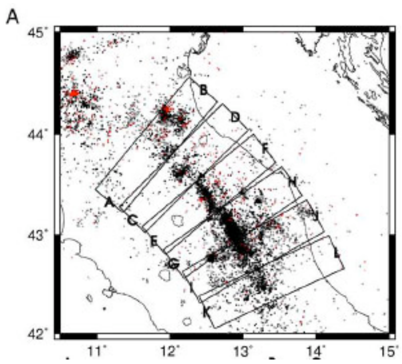

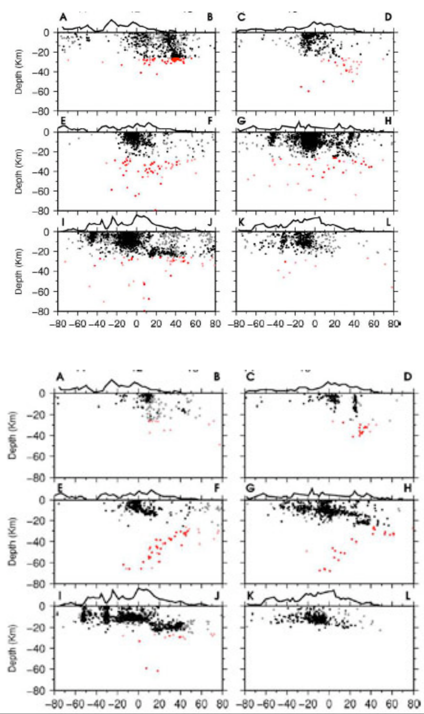

De Luca et al., 2009, Tectonophysics

UPDUCTION

(E-NE verging subduction)

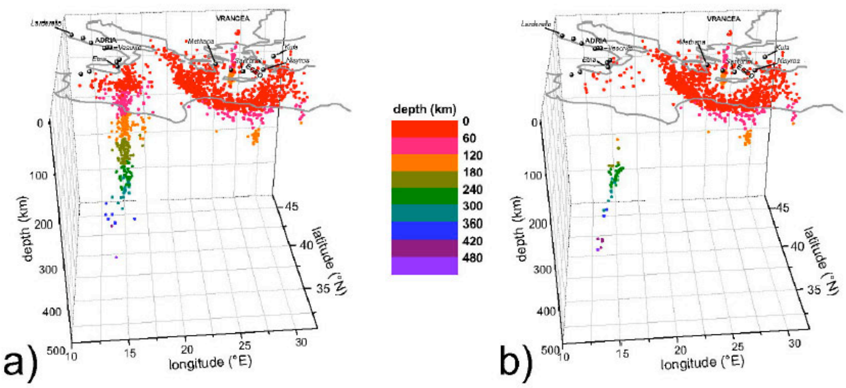

Fig. 1 – The Mediterranean is characterised by four deep earthquake spots: South Tyrrhenian, Aegean, West Turkey, Vrancea. The geographical position of the four deep foci clusters, their narrowness and azimuth are not compatible with mechanical processes linked to a very long front of subduction between Africa and Eurasia. The black circles on the surface represent the volcanoes that have erupted in historical time. a) Tyrrhenian foci from CSI-INGV catalogue and Aegeum and Vrancea from Engdahl Global Catalogue of relocated Hypocentres. b) All hypocentres from the Engdahl Global Catalogue of Relocated Hypocentres.

Scalera, 2008

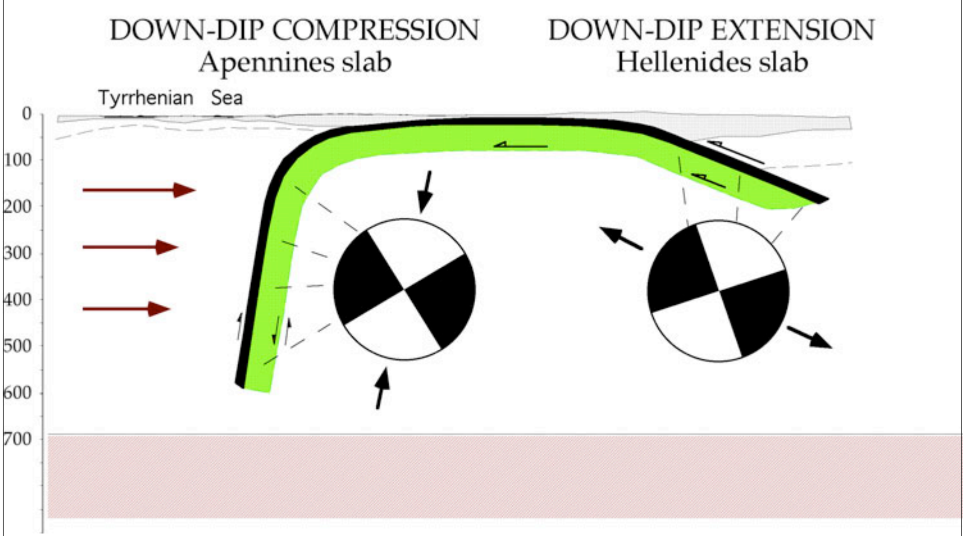

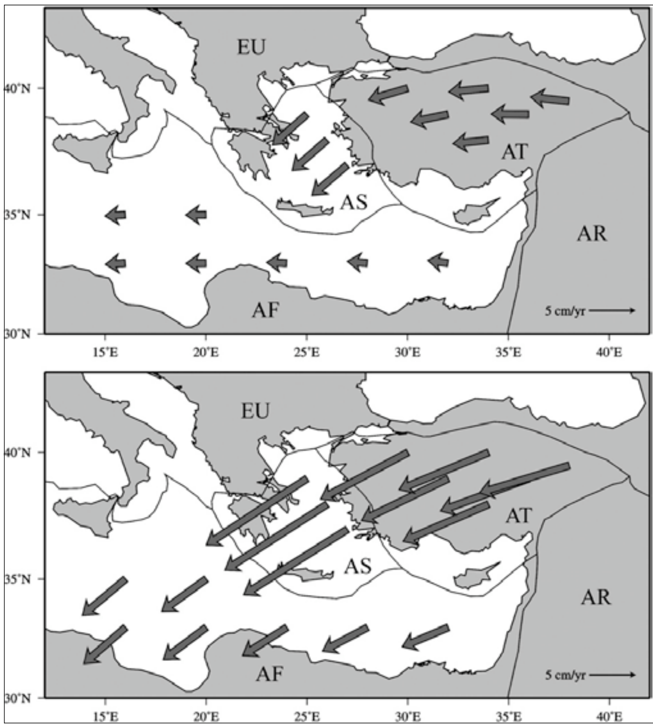

Plate motions of Africa and Greece relative to the mantle in the deep hotspot reference frame (above) and in the shallow hotspot reference frame. In both cases Africa is moving westward faster than the underlying mantle, escaping from the subduction under the Hellenic arc (Doglioni et al. 2007, Earth-Science Reviews, 83 125–175).

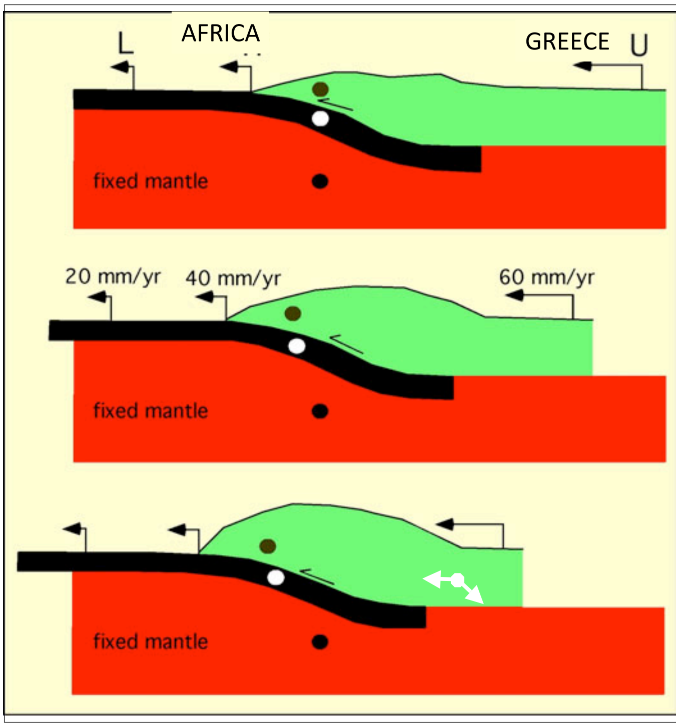

When plate motions are considered relative to the hotspot reference frame, i.e., assuming fixed the mantle, the slabs of E- or NE-directed subduction zones may move out of the mantle (upduction). In the three stages sketch the white dot moves leftward relative to the underlying black dot in the mantle. Subduction occurs because the upper plate dark gray dot moves leftward faster than the white circle in the slab. In this model, the slab moves west at 20 mm/yr relative to mantle. The subduction rate is the convergence minus the orogenic shortening. With different velocities, this seems to apply, in the shallow hotspot reference frame, also to the Andean subduction. This kinematic evidence of upducting slabs casts doubts on the slab pull as the dominant driving mechanism of plate motions. (Doglioni et al. 2007, Earth-Science Reviews, 83 125–175).

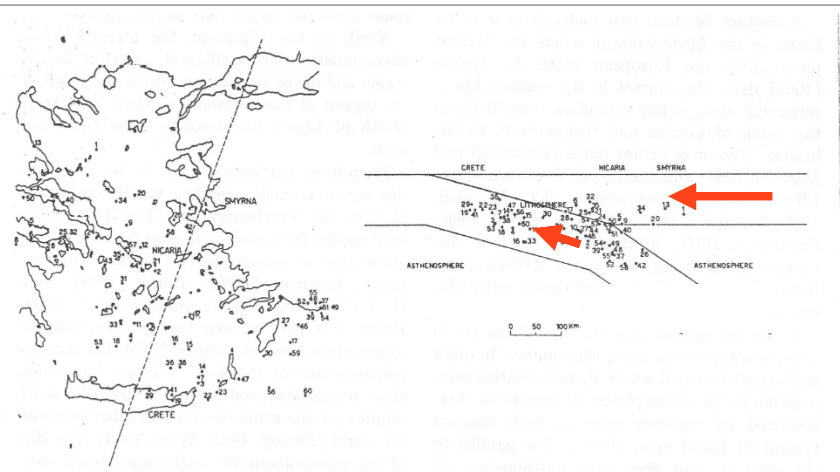

Caputo, M., Panza, G.F. and Postpischl, D., (1970). Deep structure of the Mediterranean basin. J. Geophys. Res., 75, 4919-4923 (modified).

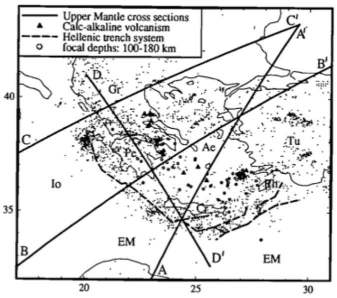

Location map of the Eastern Mediterranean and Aegean area. Thick solid lines indicate the location of Upper Mantle cross sections. Dots indicate the epicenters of earthquakes with M>4 and focal depths less than 100 km that occurred from 1964-1984. Ae=Aegean basin, Cr=Crete, EM=Eastern Mediterranean, Gr=Greece, Io=Ionian basin, Pe=Peleponnesus, Rh=Rhodes, Tu=Turkey, for remaining items see key.

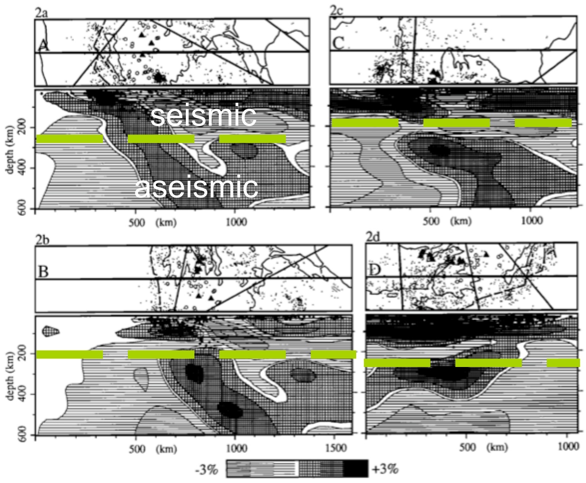

Tomographic images of the Aegean/Eastern Mediterranean Upper Mantle for the sections shown on the left (The upper panels in a-d display a small location map for orientation). The contouring is in percentages of the ambient Jeffreys-Bullen Upper Mantle velocity (see legend). Cross (horizontal) hatching indicates positive (negative) anomalies. Regions with poor spatial resolution are not contoured (large white areas). The interval -0.1%/+0.1% is also indicated in white. Horizontal and depth axes given without vertical exageration. Black symbols are the projection of hypocenters with M>4 are located within 100 km from the plane. The width of the location map is 3 degrees (Spakman, et al., 1988. THE HELLENIC SUBDUCTION ZONE: A TOMOGRAPHIC IMAGE AND ITS GEODYNAMIC IMPLICATIONS,G.R.L., 15, 60-63).

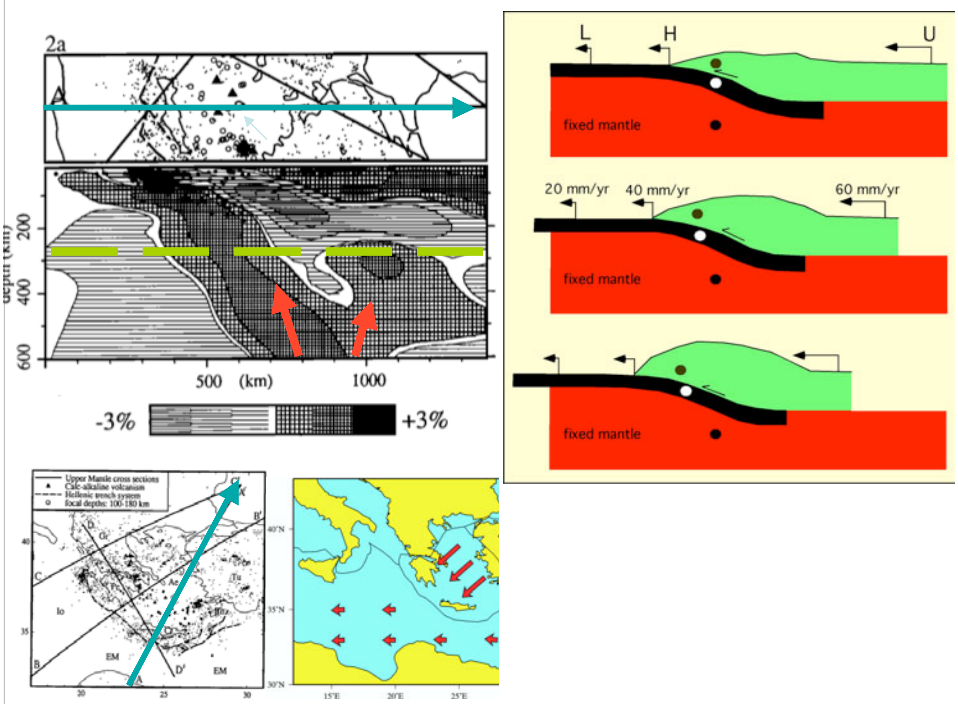

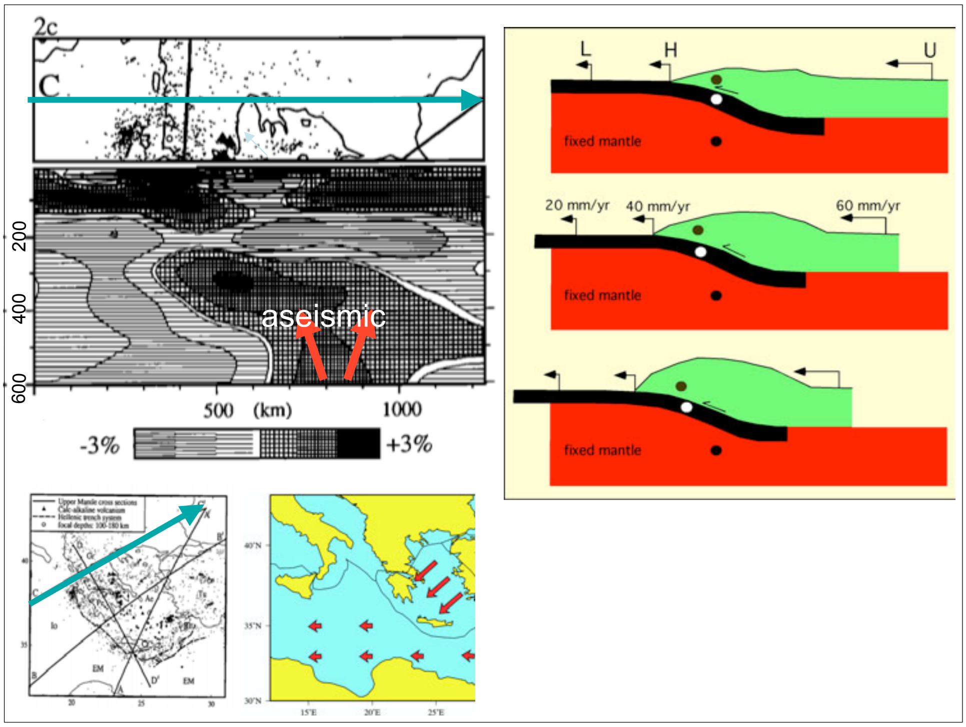
2c
C
200
400
600
aseismic
500 (km)
1000
-3%
+3%
L
H
U
fixed mantle
20 mm/yr
40 mm/yr
60 mm/yr
fixed mantle
fixed mantle

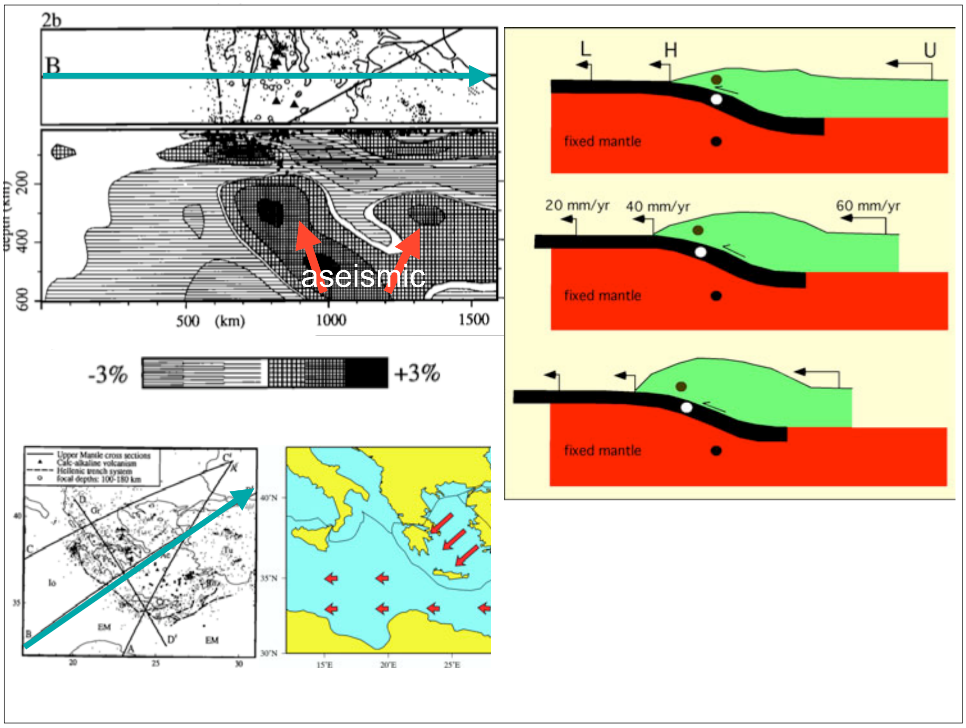
2b
B
200
400
600
aseismic
500 (km)
1000
1500
-3%
+3%
L
H
U
fixed mantle
20 mm/yr
40 mm/yr
60 mm/yr
fixed mantle
fixed mantle

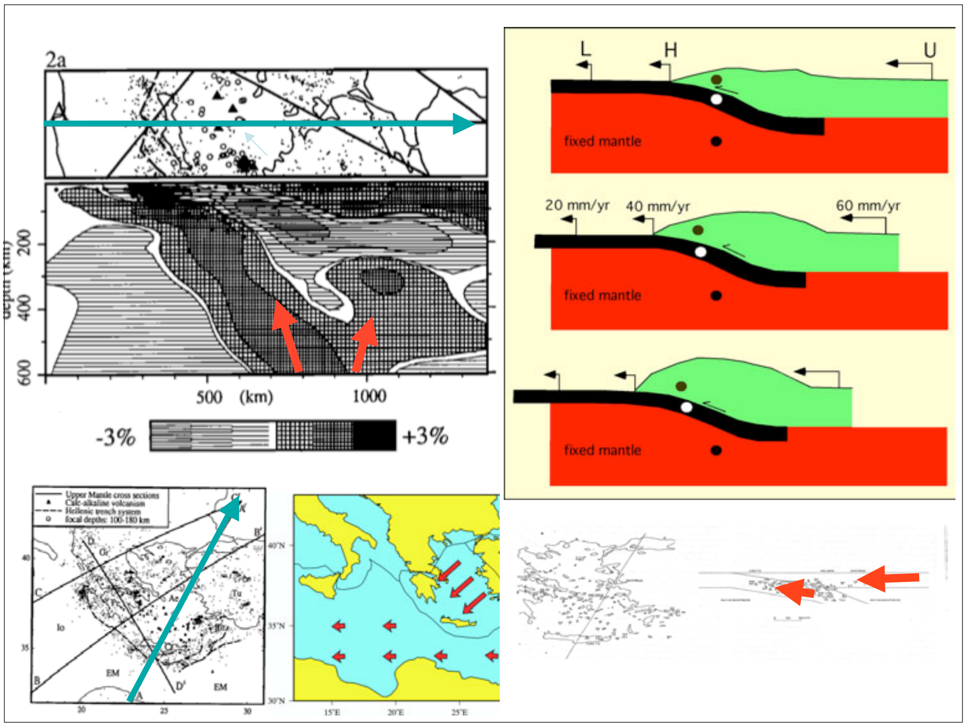

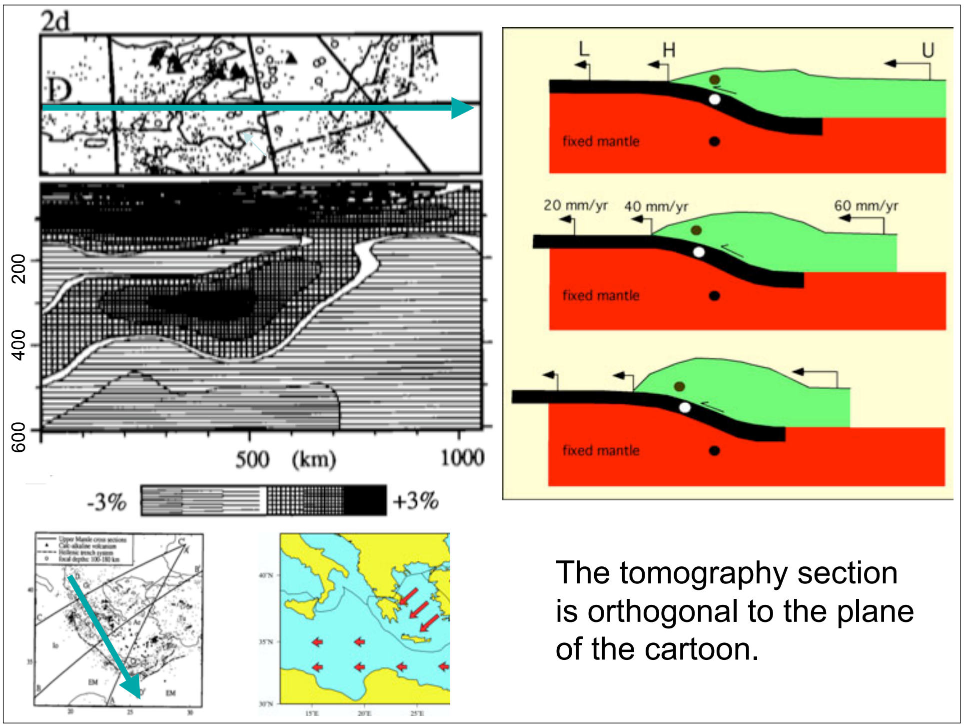

The tomography section is orthogonal to the plane of the cartoon.

Rival Models of Active Margins

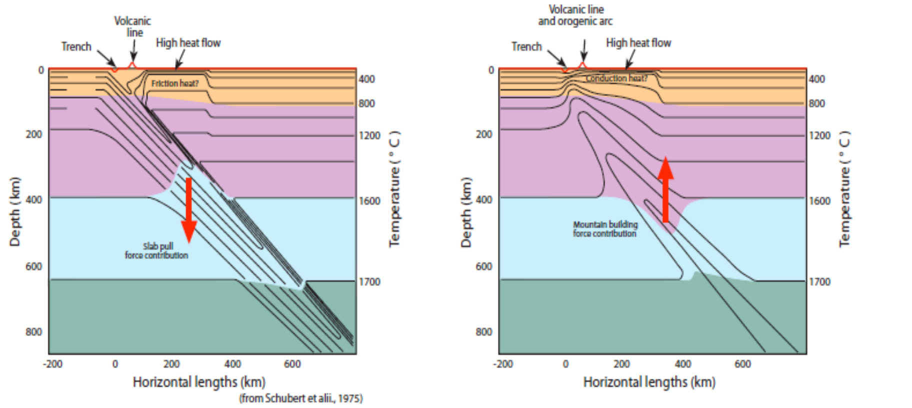

Two rival models of the active margins. Left: the subduction model is represented with the effect of the downward adiabatic transport of the isotherms. Since, at lower temperatures, the phase transformations occur at lower depths (Clapeyron slope effect), a protuberance of denser material above the 410 km discontinuity contributes to the so called “slab pull” force (retraced from Ranalli, 1995). Right: the positive anomalies of seismic velocity revealed by tomographic methods are interpreted as intrusions of isostatically upward transported material. In this case the isotherms are also transported toward the surface thus locally influencing the depth to which the phase transition occurs. This last effect is opposite to the one in the subductive model and a protuberance of lower density material is created in the denser transition zone. (Scalera, 2007)

Rival Models of Active Margins

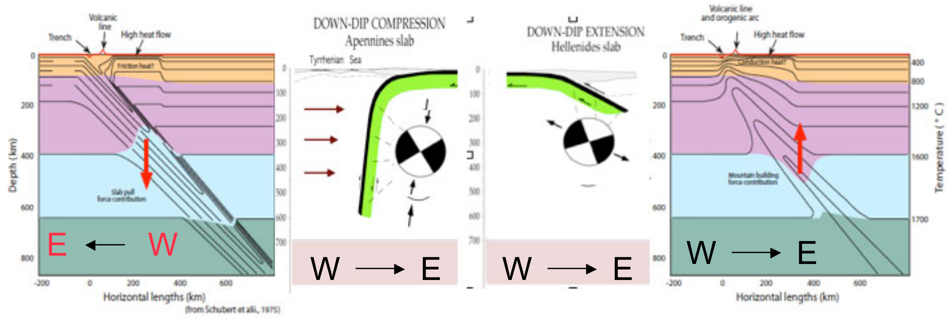

Two rival models of the active margins. Left: the subduction model is represented with the effect of the downward adiabatic transport of the isotherms. Since, at lower temperatures, the phase transformations occur at lower depths (Clapeyron slope effect), a protuberance of denser material above the 410 km discontinuity contributes to the so called “slab pull” force (retraced from Ranalli, 1995). Right: the positive anomalies of seismic velocity revealed by tomographic methods are interpreted as intrusions of isostatically upward transported material. In this case the isotherms are also transported toward the surface thus locally influencing the depth to which the phase transition occurs. This last effect is opposite to the one in the subductive model and a protuberance of lower density material is created in the denser transition zone. (modified from Scalera, 2007)

Rival Models of Active Margins

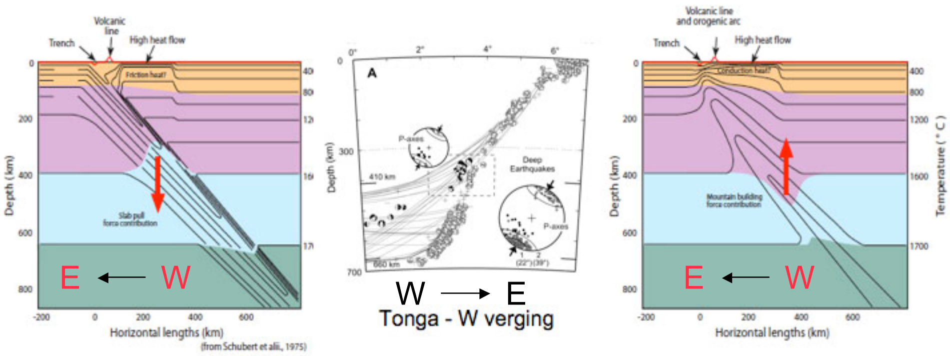

Two rival models of the active margins. Left: the subduction model is represented with the effect of the downward adiabatic transport of the isotherms. Since, at lower temperatures, the phase transformations occur at lower depths (Clapeyron slope effect), a protuberance of denser material above the 410 km discontinuity contributes to the so called "slab pull" force (retraced from Ranalli, 1995). Right: the positive anomalies of seismic velocity revealed by tomographic methods are interpreted as intrusions of isostatically upward transported material. In this case the isotherms are also transported toward the surface thus locally influencing the depth to which the phase transition occurs. This last effect is opposite to the one in the subductive model and a protuberance of lower density material is created in the denser transition zone. (Scalera, 2007)

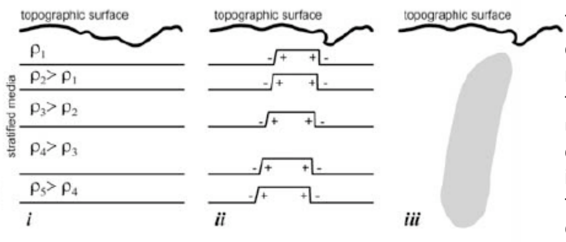

ρ_i indicates elastic parameters, density and their ratio

a

The internal pressure and isostasy drives the vertical rising of deep mantle material along the wake left by the upducting slab. If the previously undeformed stratified media ***i*** has density and velocity functions increasing toward the Earth's center, the rising column in ***ii*** produces a contrast (represented as faced '–' and '+' in ***ii***) that the seismic tomography, represented in ***iii***, can interpret erroneously in a different way: a cold downgoing slab.

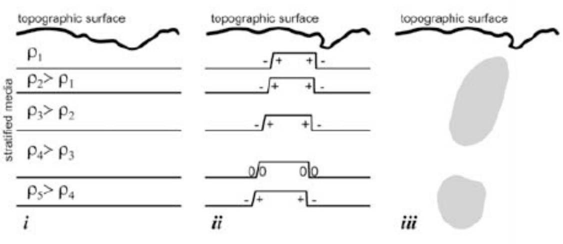

b

Scalera, G., 2005, modified

If, for example, in the fourth layer the rising column in ***ii***, because of a difference in decompression or depletion of fluids, reaches a state in which the resulting elastic parameters produce a null velocity contrast (faced '0' and '0' in ***ii***) and consequently the slab-like continuity appears broken in the tomography represented in ***iii***. Such a situation can be erroneously interpreted as a detached slab which is dropping toward the deep mantle.

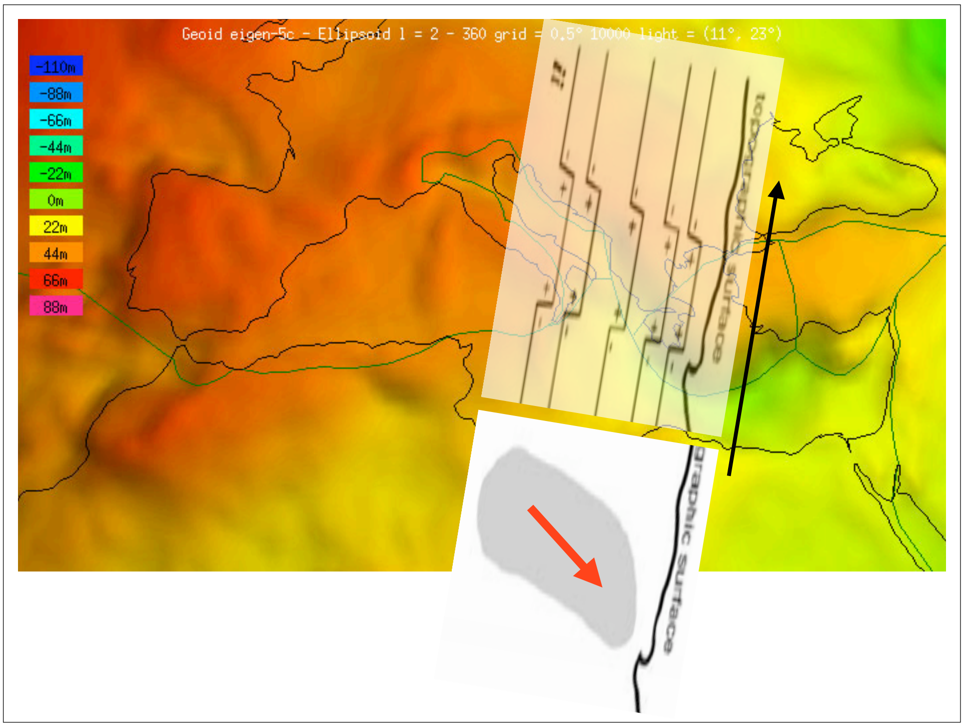

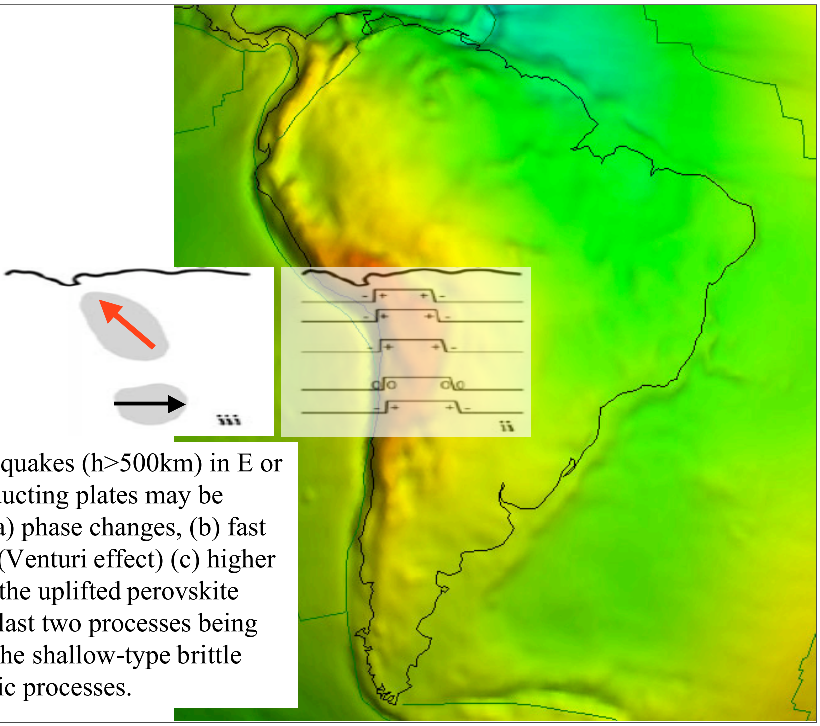

Deep earthquakes (h>500km) in E or E-NE subducting plates may be linked to (a) phase changes, (b) fast strain rate (Venturi effect) (c) higher rigidity of the uplifted perovskite phase, the last two processes being similar to the shallow-type brittle seismogenic processes.

Rifts
are not symmetric at depth

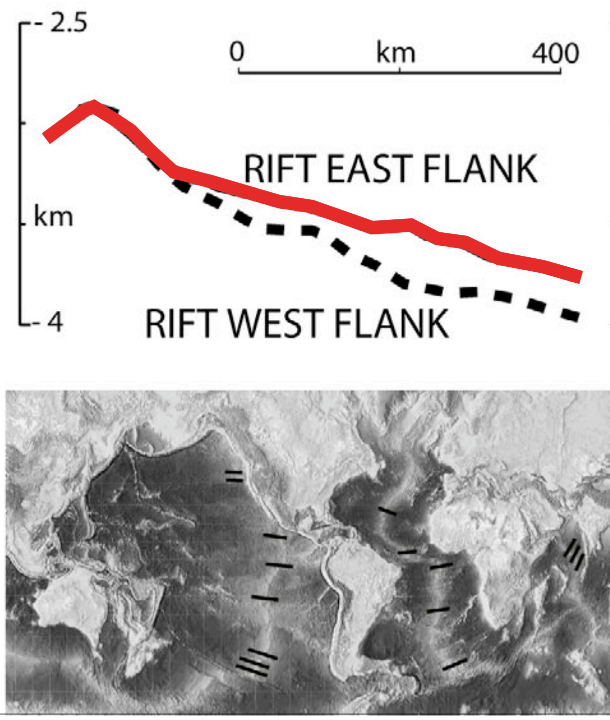

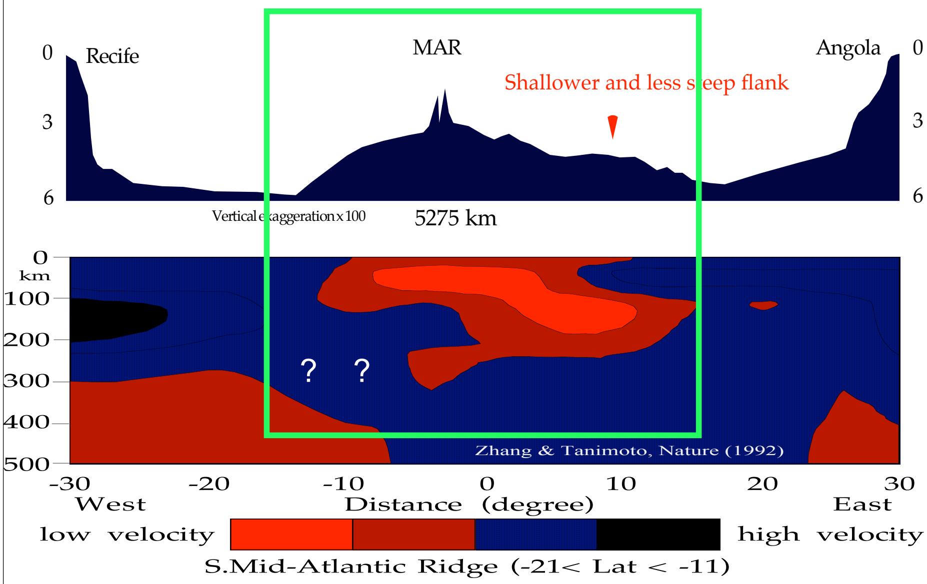

modified

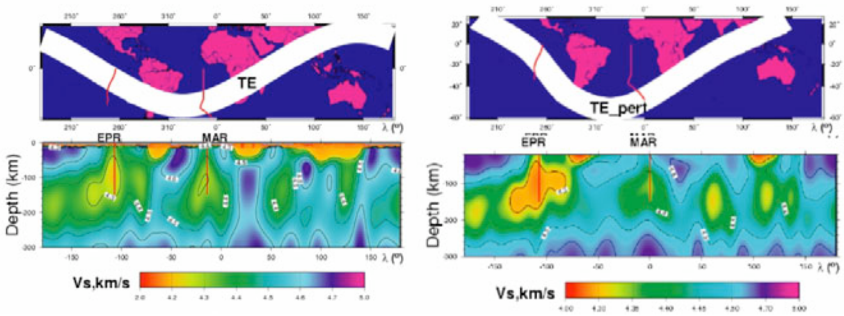

Panza, Doglioni & Levshin, 2009, in progress

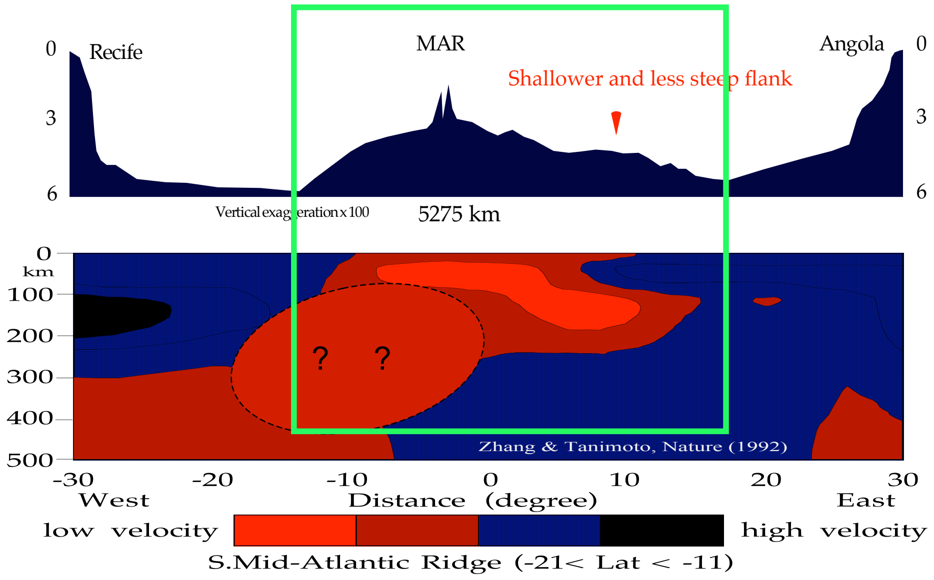

modified

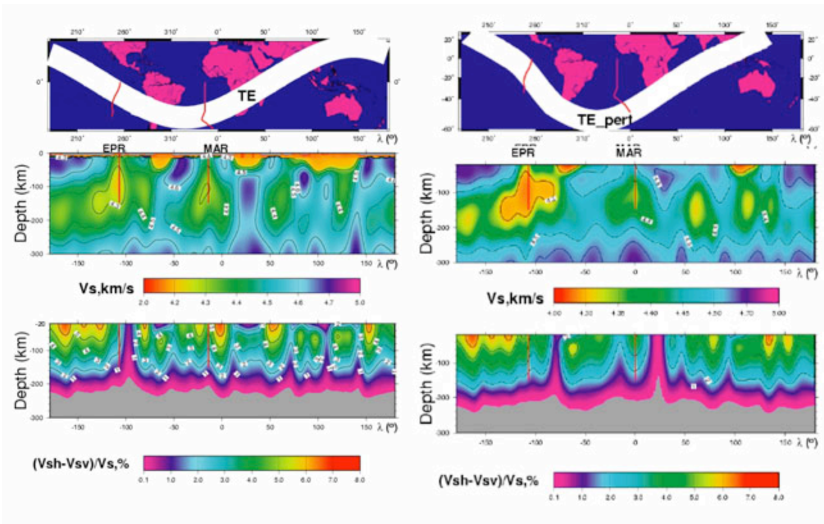

Panza, Doglioni & Levshin, 2009, in progress

From Mundus Subterraneus, by Athanasius Kircher, 1678.

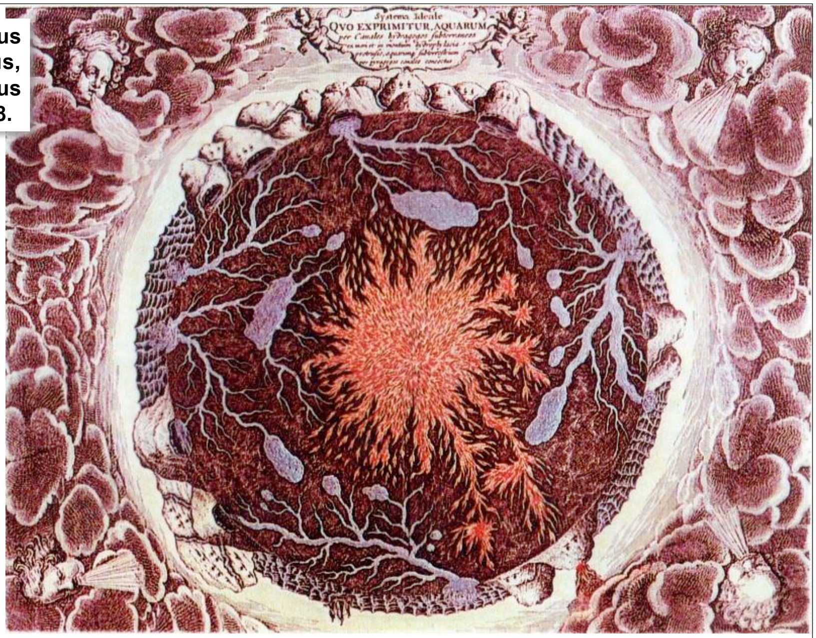

Athanasius Kircher, depicted the most advanced thinking of his day. Earth's interior was supposed to contain a giant, fiery inferno.

The fires heated water that had seeped in from the ocean and gave rise to hot springs. Where tongues of fire came close to Earth's surface (lower right), they started volcanoes.

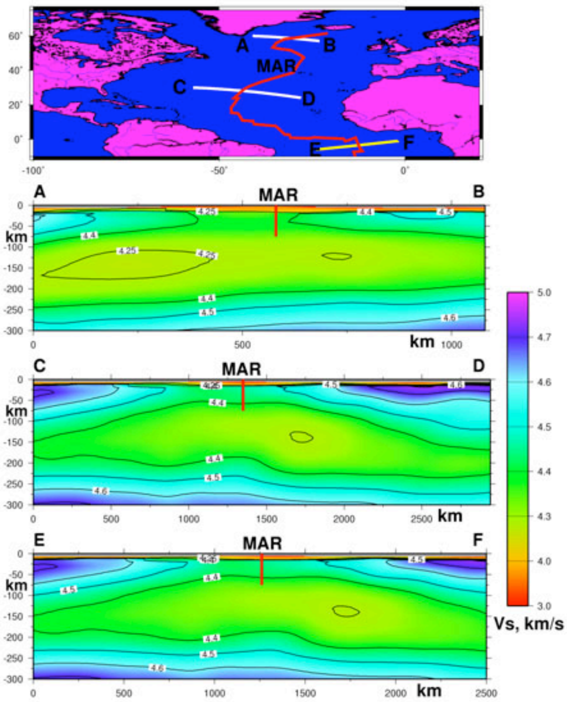

Cartoon of an oceanic rift with hypothetic velocities of plates a and b relative to a fixed mantle. The ridge moves west at the velocity Vr. The separation between plates triggers the uplift of undepleted mantle previously located to the west. In the melting area, the mantle looses Fe, Mg, and other minerals to form oceanic crust, while the residual mantle is depleted. Since the melting area moves west it gradually transits towards the undepleted mantle, releasing to the east a depleted mantle. This explains the slight shallower bathymetry of the eastern limb and can generate the asymmetry of seismic waves velocity seen before.

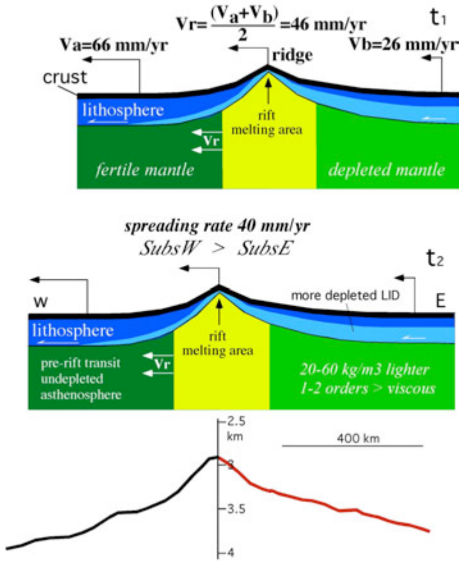

In this model, the differential velocity among plates is controlled by LVZ viscosity variations generating variable decoupling between lithosphere and mantle. (Doglioni et al., 2005; 2009)

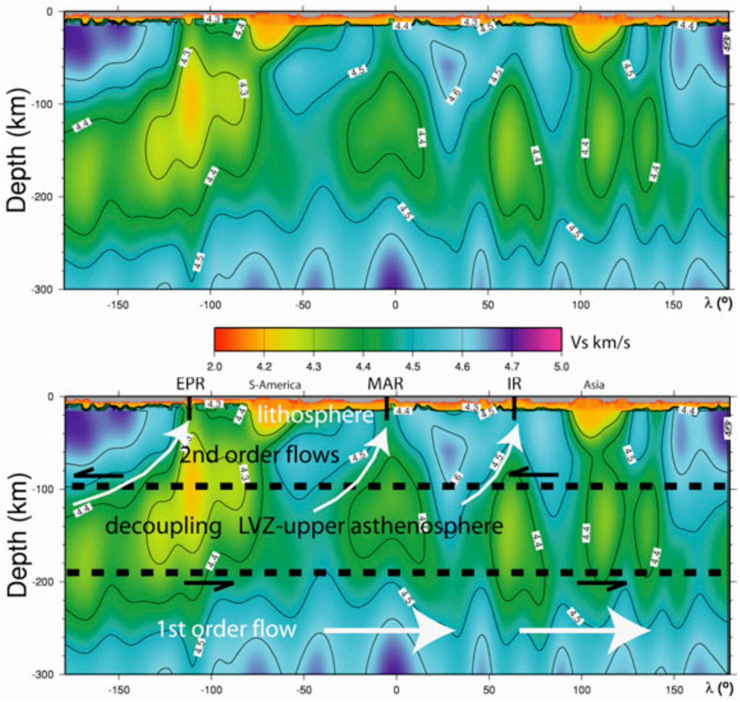

Panza, Doglioni & Levshin, 2009, in progress

What drive tectonics ?

Current hypothesis

- only Earth's cooling:

classical convection
or
slab pull

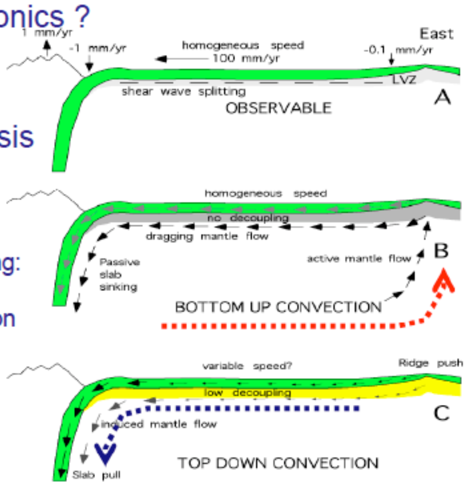

Doglioni et al., 2007

unconventional hypothesis

•combined effect of Earth's cooling, Earth's rotation and tides acting on decoupled layers

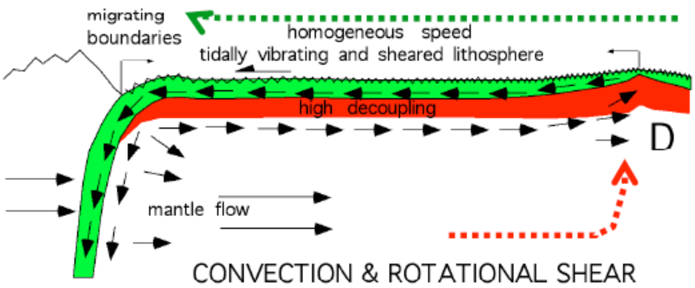

Doglioni et al., 2007

The lithosphere-asthenosphere system in the Mediterranean region and westward mantle flow

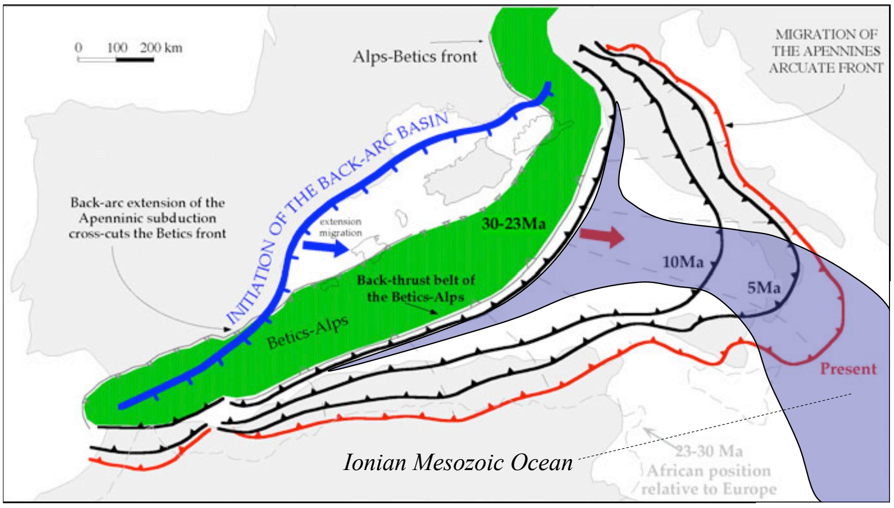

E-ward slab retreat
5 times faster than N-S convergence

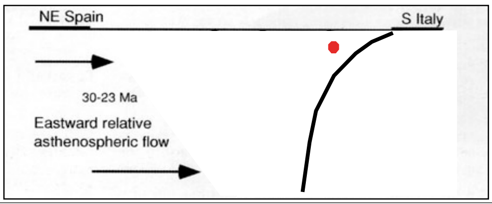

3D model of Vrancea

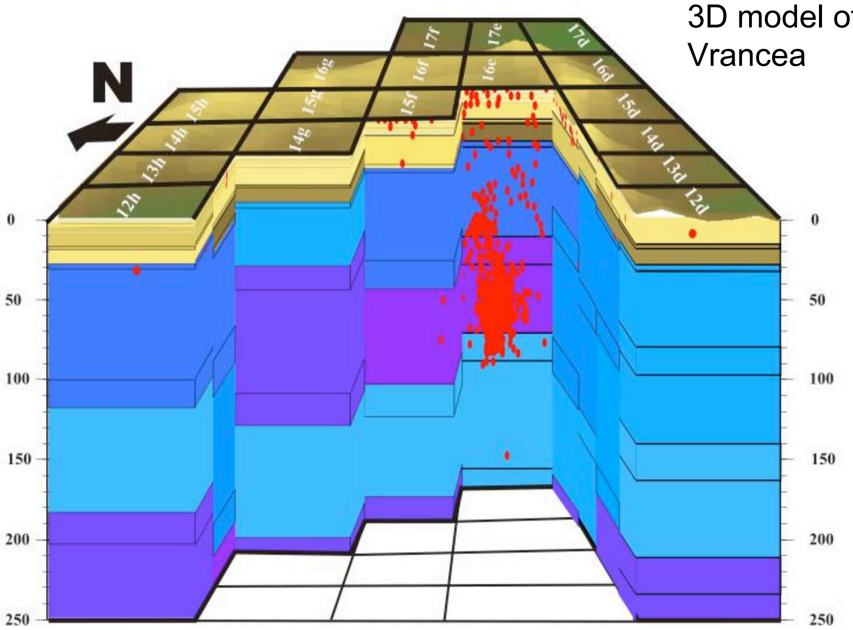

(Raykova and Panza, PEPI 2006)

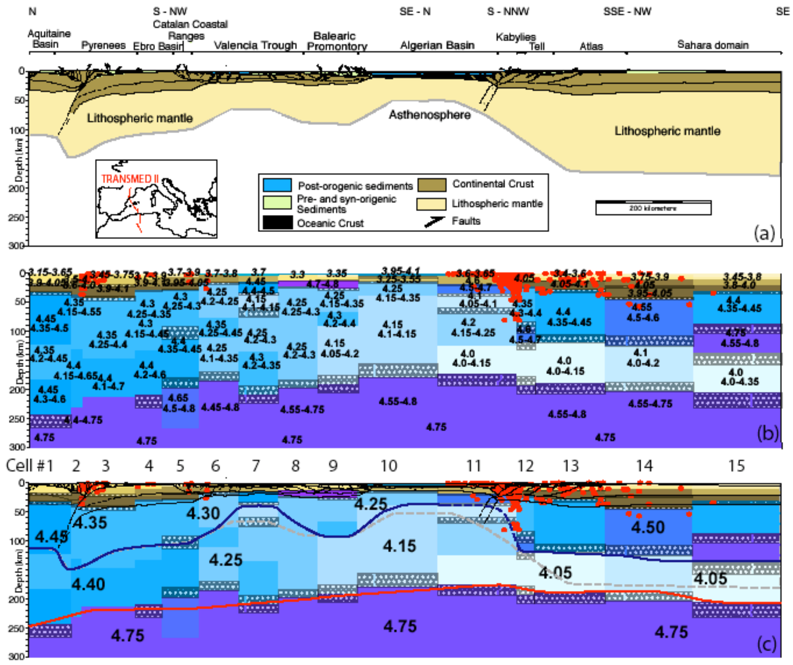

(Panza et al., EPSL, 2007)

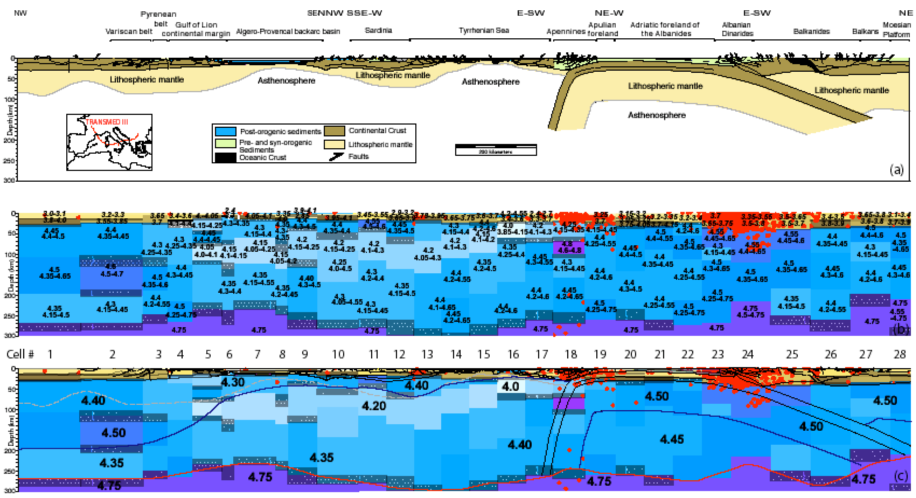

(Panza et al., EPSL, 2007)

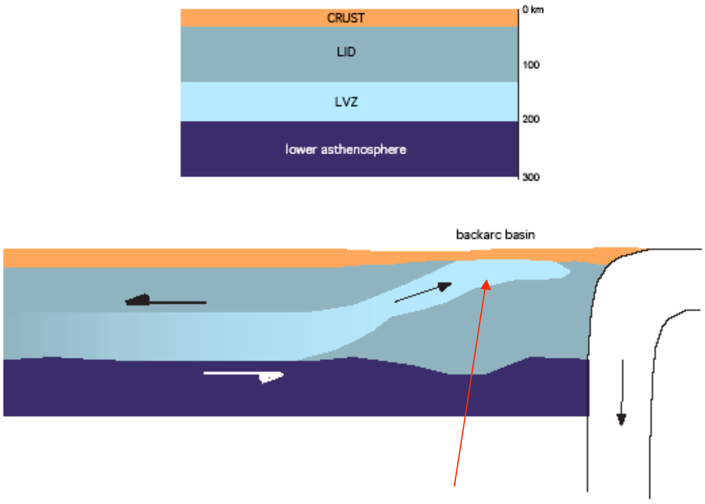

splash of mantle: volcanoes

(Panza et al., EPSL, 2007)

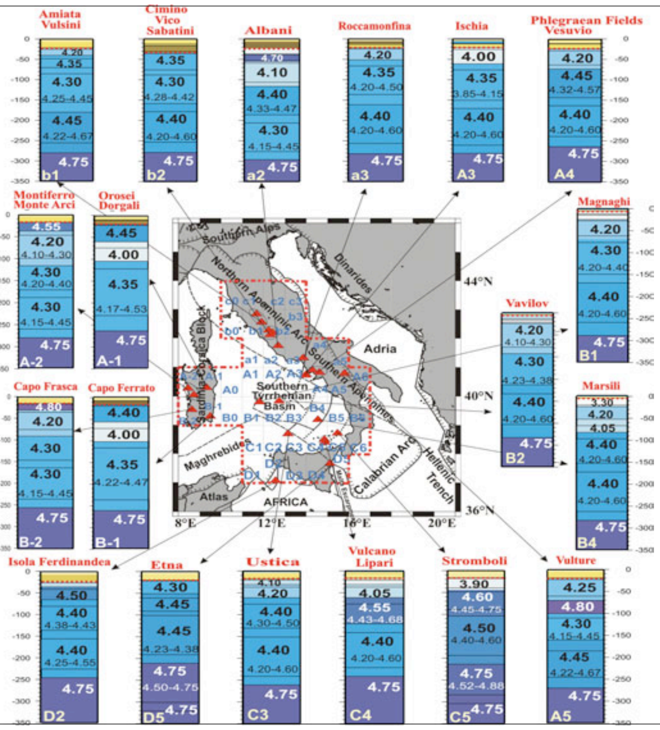

Plio-Quaternary magmatic provinces in Italy.
Modified after Peccerillo and Panza (1999)

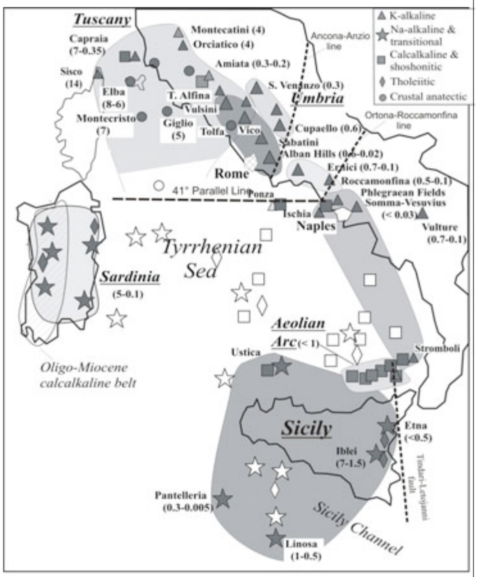

The largest Volcanic risk in the world

VESUVIUS

Cartoon showing the three-dimensional geodynamic scheme of the Tyrrhenian basin and bordering volcanic areas, including the subduction of the Ionian-Adria lithosphere in

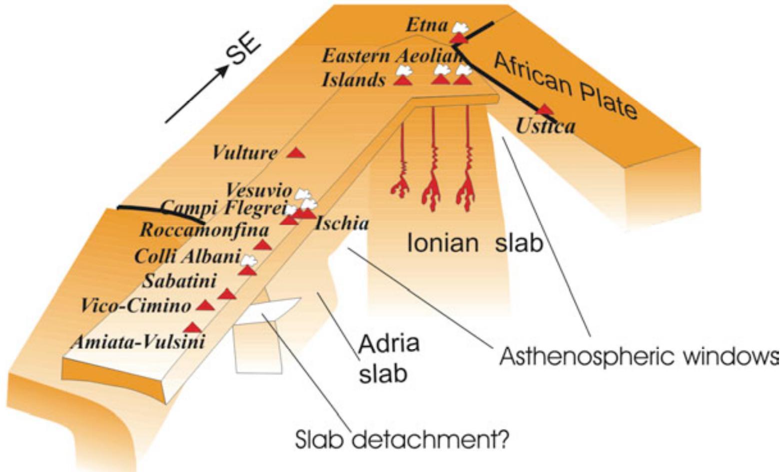

Mt. Vesuvius cone

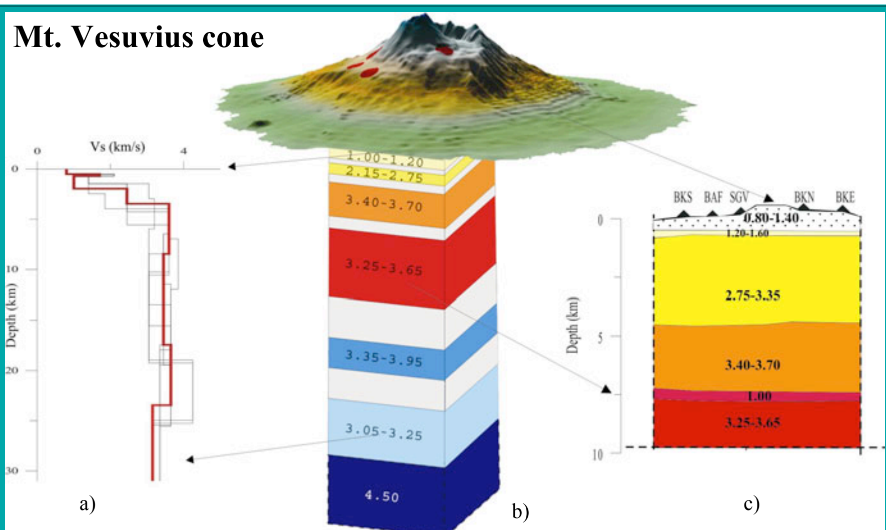

(a) Hedgehog solutions (lines) from the average Rayleigh wave group velocity dispersion curve computed, in the period range 0.3-2 s, for all stations on **Mt. Vesuvius cone** (BAF, BKN, BKS, BKE, SGV), and regional group (T=10-35s) and phase (25-100s) velocities.
(b) The chosen Vs models are shown along SE-NW-SW-NE cross-sections through Somma-Vesuvius. The grey bands indicate the boundaries between layers, that can well be transition zones in their own right, and the group of numbers indicate the ranges for V_S in km/s.
(c) Uppermost part of the chosen model, if we impose, as a priori information, the value of 1.0km/s (Auger et al., 2003), for the low velocity layer at 8km of depths (this ultralow-velocity layer is present in all solutions).

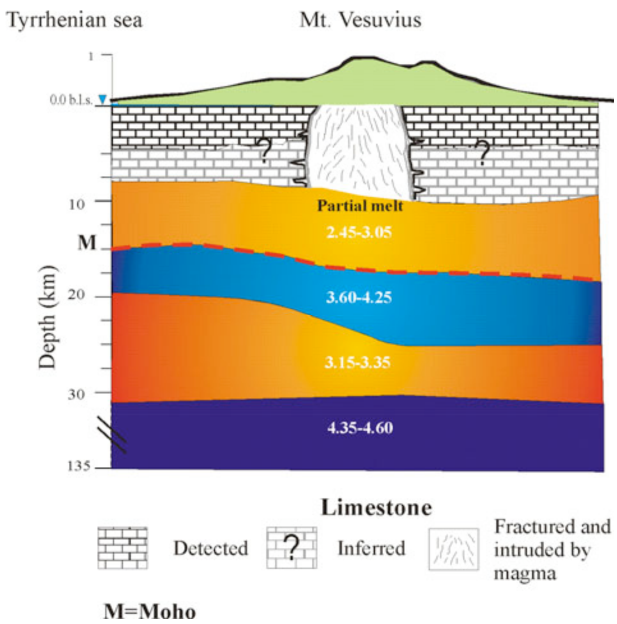

Schematic model of the crust and uppermost mantle at Mt. Vesuvius. The possible ranges of Vs are given in the figure while the uncertainty (about 1-2 km) of the thickness for each layer is omitted for clarity reasons. The Moho depth (M) is shown as dashed line.

Comparison between Campi Flegrei and Vesuvian structural models

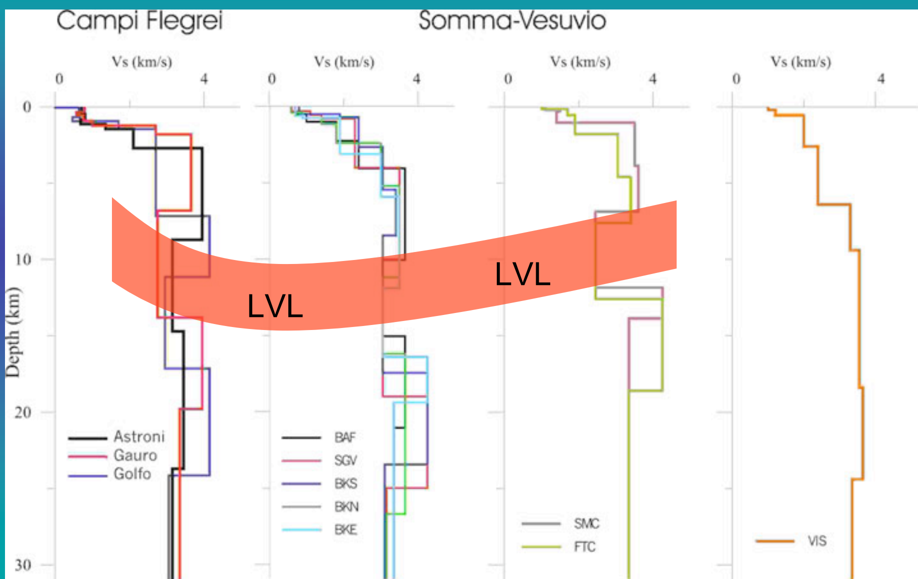

Map of Campi Flegrei and Vesuvio volcanic areas

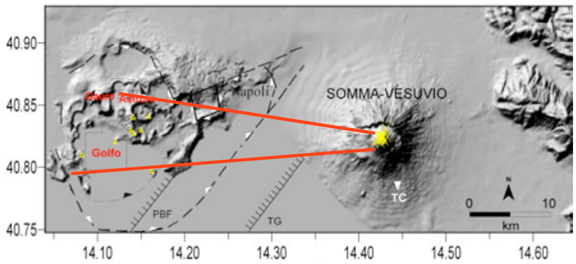

Vs models along a SW-NE cross-section through the Vesuvio-Campi Flegrei paths. The grey bands indicate the boundaries between layers, that can well be transition zones in their own right.

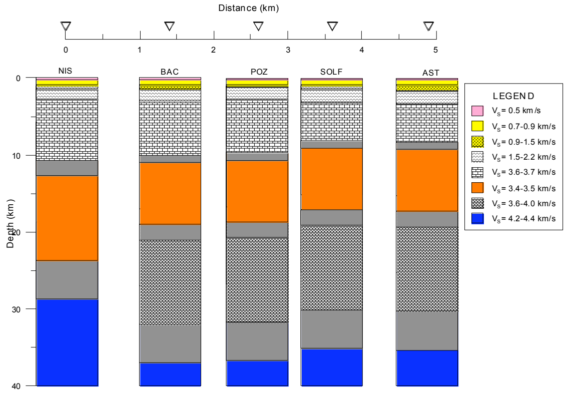

Nunziata, 2009, in press

CO_2 mantle degassing

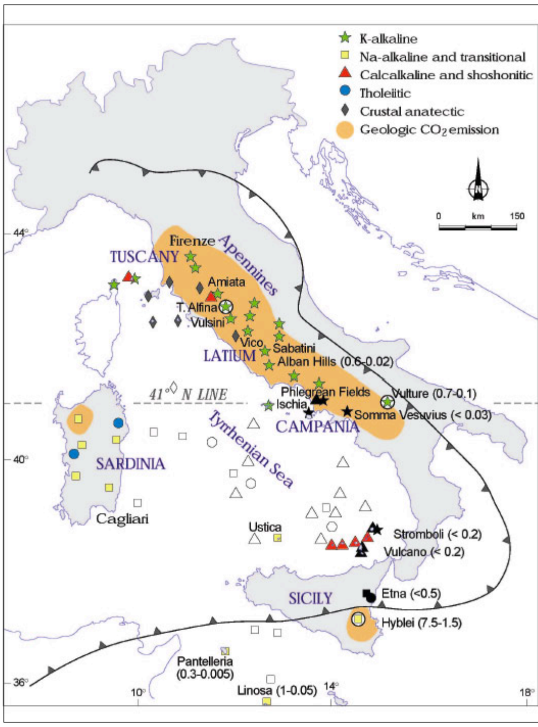

Distribution of main geological CO_2 emission in Italy (orange area), as derived from the online catalogue of Italian gas emissions,(http://googas.ov.ingv.it), and of petrochemical affinities and ages of the main Plio-Quaternary magmatic centers in Italy. Active volcanoes are marked in black. Ages in parenthesis. (modified from Peccerillo, 2005)

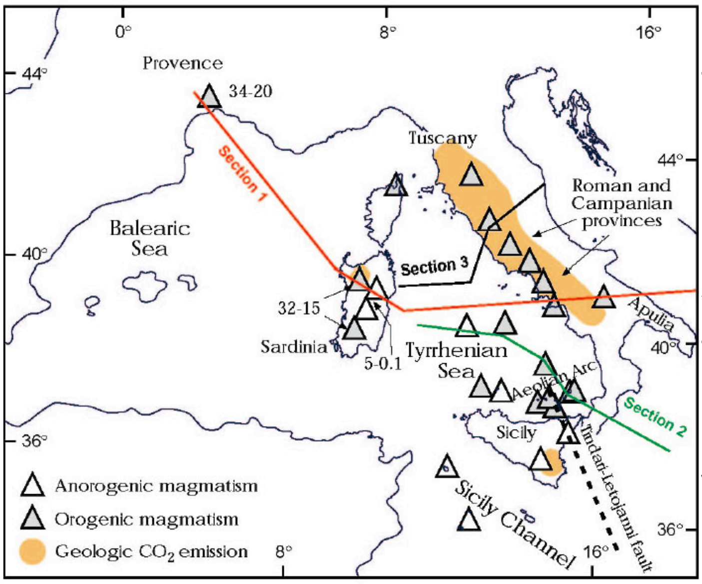

Location of the orogenic and anorogenic Plio-Quaternary volcanism in the Western Mediterranean (from Peccerillo, 2003), with respect to geological CO_2 emission areas.

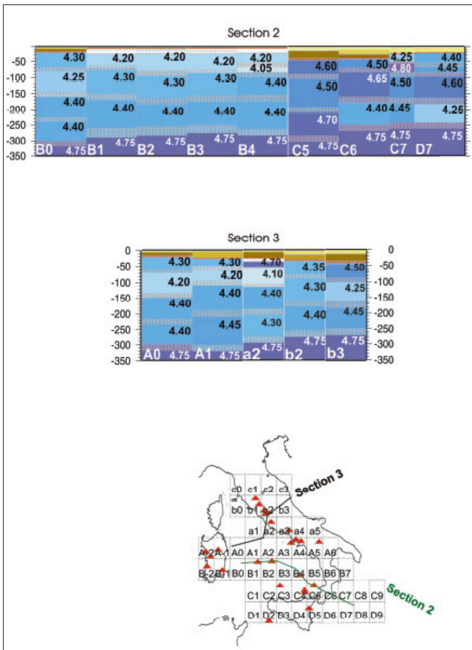

Vs models of the lithosphere-asthenosphere system along other representative sections in the Western Mediterranean, built from the cellular Vs model of the Tyrrhenian Sea and surroundings given by Panza et al. (2007b). In each labeled cell, the hatched zone stands for the thickness variability, while, to avoid crowding of numbers, only the average shear velocity is reported. The Vs ranges of variability are given in Panza et al. (2007a). Red triangles indicate recent and active volcanoes.

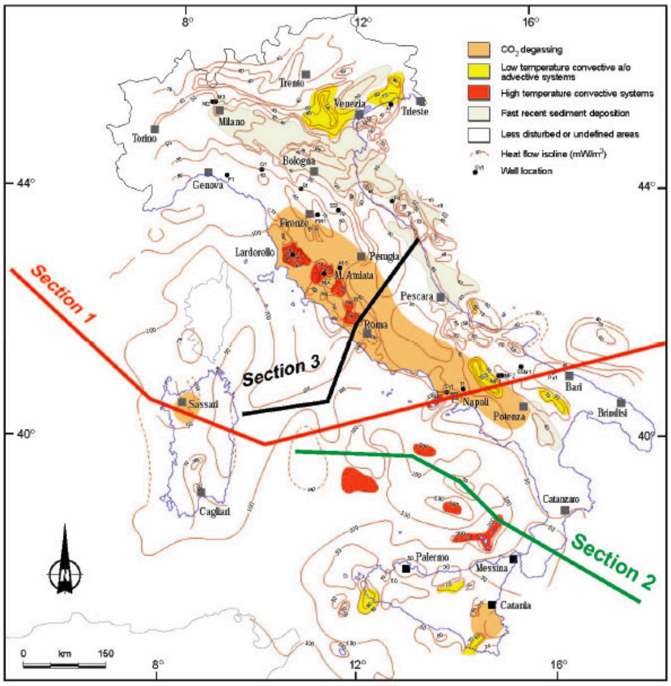

Heat flow map of Italy reporting the location of major CO_2 degassing areas. Most non-volcanic CO_2 emission occurs in areas of normal heat flow. Local high heat flow is associated with subsurface magmas and includes CO_2 fluxes from major geothermal systems (Larderello and Monte Amiata, in Tuscany). Numbered lines represent the pathway of sections just illustrated.

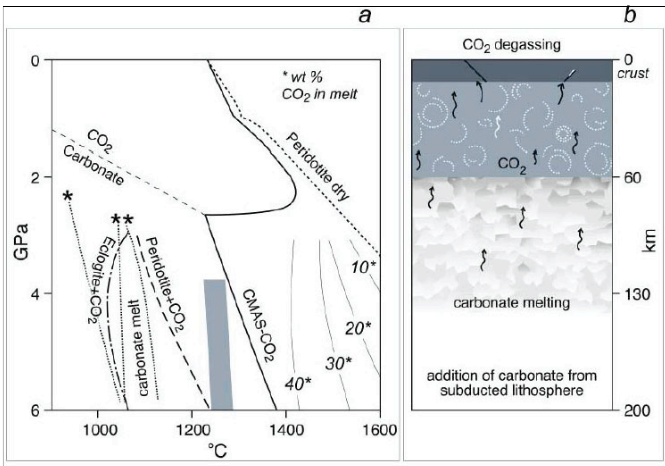

Lithosphere - asthenosphere degassing beneath the Western Mediterranean.
a) Pressure-temperature diagram showing the effects of CO2 on the *solidus* of carbonated lithologies in the mantle: CMSA - CO2, and peridotite - CO2 (2.5 wt %). The effect of carbonates on the composition of melts generated at increasing temperature is reported as wt% CO2. Gray area = estimated present-day mantle temperatures at the inferred pressures.

b) Present mantle processes and metasomatism beneath the Western Mediterranean. Melting of sediments and/or continental crust of the subducted Adriatic-Ionian (African) lithosphere, generates carbonate-rich (hydrous-silicate) melts at P > 4 GPa (130 km) and T > 1260°C. Due to their low density and viscosity, such melts can migrate upward through the mantle, forming a 70 km thick carbonated partially molten CO2-rich mantle layer recorded by tomographic images. Upwelling of carbonate-rich melts to depths less than 60 - 70 km, induces massive outgassing of CO2 in the lithospheric mantle, with cessation of Vs attenuation. Buoyancy forces, probably favored by fluid overpressures, and tectonics might allow further CO2 upwelling to the Moho and the lower crust, and, ultimately, outgassing at the surface.

Earthquake prediction and non-linear dynamics

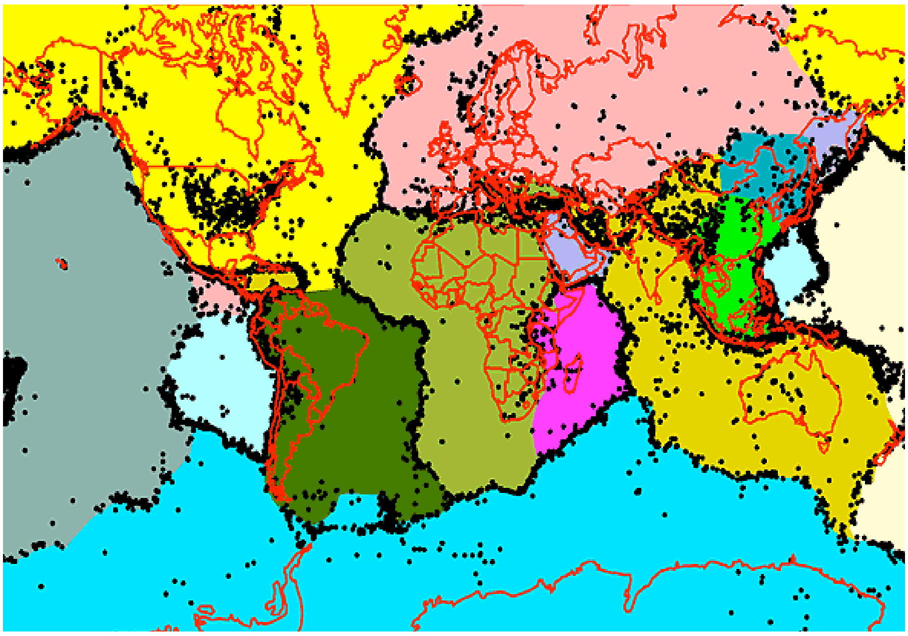

Earthquakes and lithospheric plates

Characteristics of the lithosphere

Scale invariance of earthquake distribution in time and space

Self-organization of earthquake occurence

Non-linear mechanics of earthquake generation

Statistical features of earthquake sequences

Strongly suggest that the lithosphere behaves as a non-linear and possibly deterministic chaotic system (Keilis-Borok, 1990).

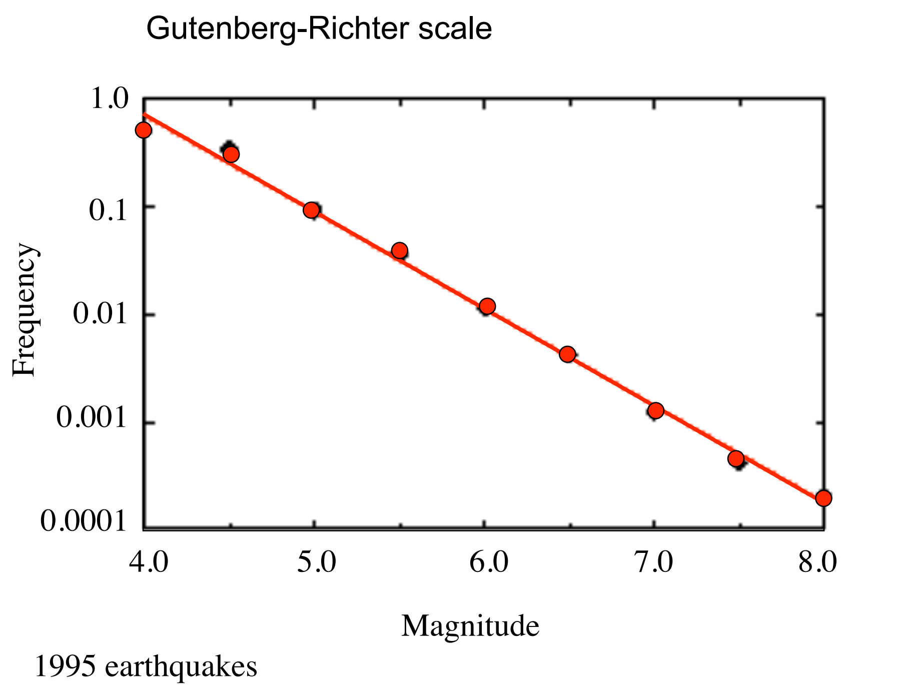

The Gutenberg-Richter log-linear law supports that the whole lithosphere is a self-organized system in critical state, i.e., a force is acting contemporaneously over all the plates and distributes the energy over the whole lithospheric shell, a condition that can be satisfied only from a force acting at the astronomical scale (e.g. tidal drag).

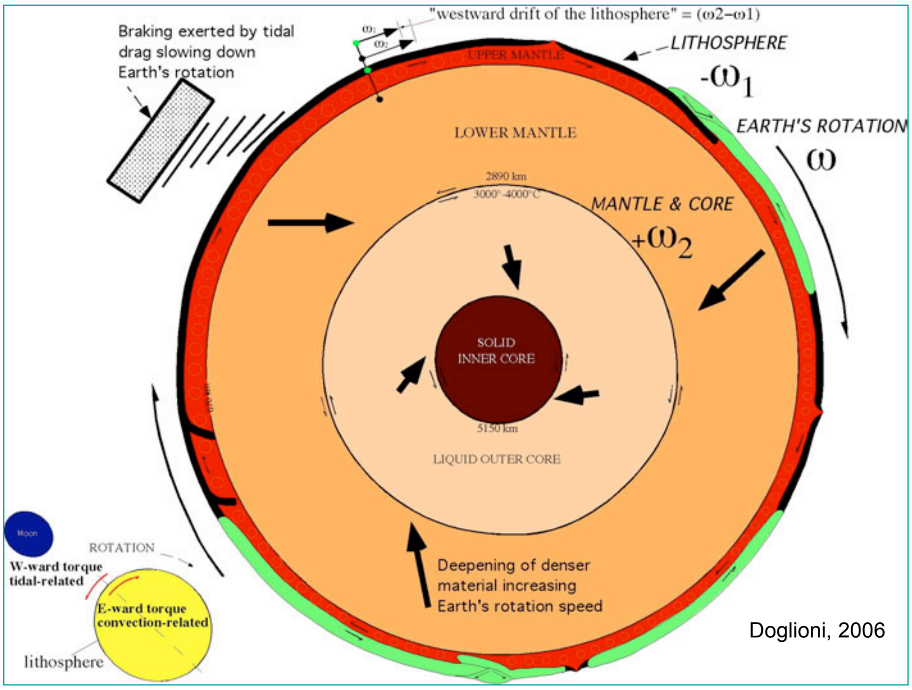


DIALOGO
DI
GALILEO GALILEI LINCEO
GR.DVCA DI TOSCANA.
MASSIMI SISTEMI DEL MONDO

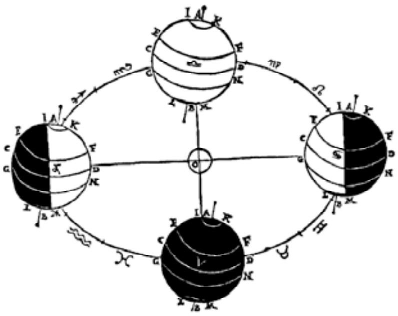

Earth tides are used by Galileo to prove the double motion of the Earth.

DIALOGO, IV giornata

The Gutenberg-Richter law

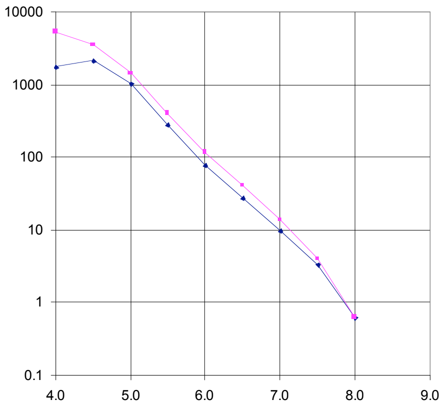

Averaged over a large territory and time the number of earthquakes equal or above certain magnitude, N(M) scales as:

$$\log_{10}N(M) = a\text{-}bM$$

This general law of similarity establishes the scaling of earthquake sizes in a given space time volume but gives no explanation to the question how the number, N, changes when you zoom the analysis to a smaller size part of this volume.

The Gutenberg Richter law when applied to small (about 200 km in length) regions is linear only over a small magnitude interval [3-4.5].

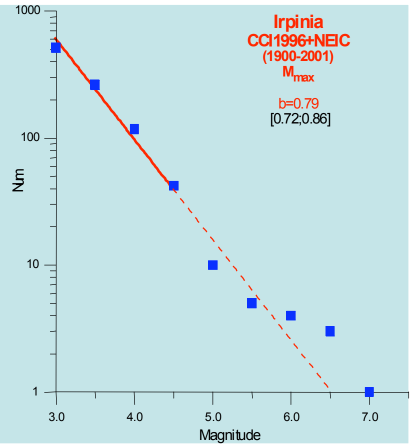

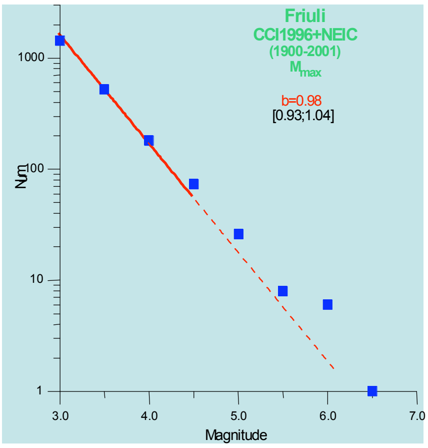

(cumulative distribution)

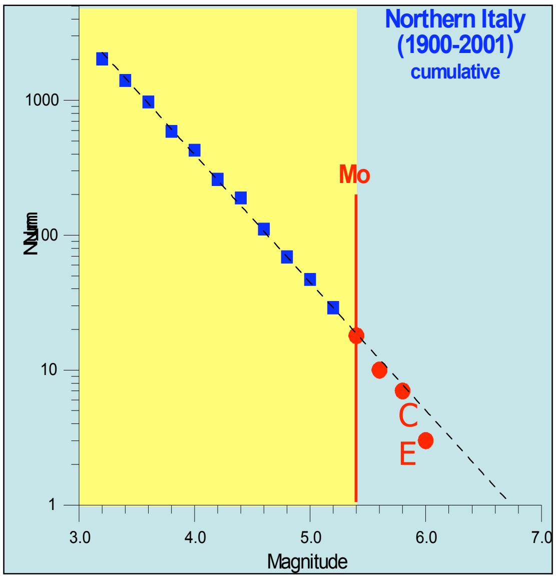

The Gutenberg Richter law when applied to larger (about 500 km in length) regions is linear over the magnitude interval [3-5.4].

The GR law for the entire Italian territory follows a linear trend over the magnitude interval [3-6.7].

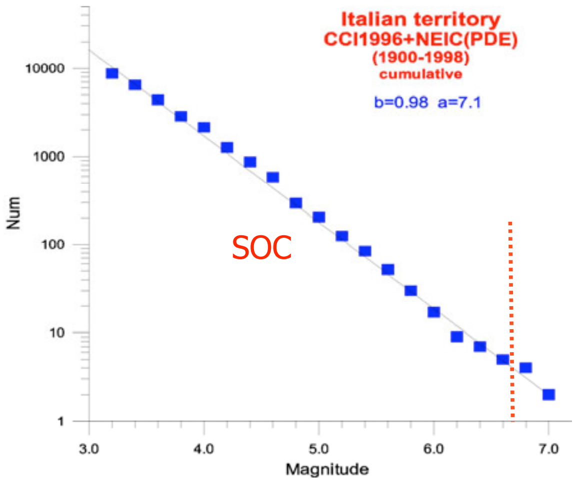

A single GR is not valid for all areas. This fact opens the way to prediction (a SOC system is not predictable) and at the same time casts doubts on the validity of the currently used procedures for the probabilistic assessment of seismic hazard.

Seismic hazard

- The multiscale seismicity model, suggested by *Molchan et al*. (1997) for the purpose of seismic hazard assessment, indicates that:

Seismic hazard

- only the ensemble of events geometrically small, compared with the elements of the seismotectonic regionalization, can be described by a Gutenberg-Richter law;
- therefore the seismic zonation must be performed at several scales with corresponding Gutenberg-Richter laws and magnitude ranges.

Intermediate-term Intermediate-range earthquake prediction

Uncertainty:

Time: a few years

Space: a few hundreds kilometres


CHIESA PARROCCHIALE
DI
SAN BIAGIO IN COSINA
DIOCESI E COMUNE DI FAENZA
(PROV. DI RAVENNA)

li 15 settembre 1950

Certifico io sottoscritto che Giuliano Panza di Giuseppe e di Giuseppina Liverani nato a S. Biagio il 27 aprile 1945 ad ore 7.15 fu Battezzato a questo S. Fonte il 23 aprile 1945 dal M. R. D. Giuseppe Bersani essendo madrina la sig. Lolli Colomba in Liverani.

Tanto risulta dai registri dei Battezzati esistenti in questo Archivio Parrocchiale, pag. 15 n. 43

L. ✠ S.

IL PARROCO
Giuseppe Bersani

Curia Vescovile di Faenza

li

Visto per l'autenticazione della firma del M. R.

IL CANCELLIERE

L. ✠ S.

My earliest credential about prediction

This is my certificate of baptism, drafted on September 15, 1950, stating that I was **born** on April **27**, 1945 and I was **christened** on April **23**,1945

Intermediate-term earthquake prediction

- A family of intermediate-term earthquake prediction algorithms has been developed on the basis of the understanding that the seismically active lithosphere has to be regarded as a hierarchical non-linear (chaotic) dissipative system, as well as by the application of pattern recognition techniques.

- **In agreement with the Multiscale approach, inside the monitored regions, the linearity of the GR is preserved only for magnitudes not larger than M_o**

- **Prediction Algorithms (CN and M8) are based on the formal analysis of the anomalies in the flow of the seismic events that follow the GR law, and predict the strong events ($M>M_0$) that are rare and do not follow GR inside the delimited region**

Intermediate-term earthquake prediction

- Some changes are observed in the earthquake's flow before a large event: it becomes more intensive and more irregular in space and time, clustering of events and long-range interaction increase.
- These changes are akin to the general symptoms of instability of many non-linear systems before collapse.

Intermediate-term earthquake prediction

- In particular, the response to a perturbation increases, becomes more chaotic and acts at long distances.
- In the case of seismicity the non-linear system is the system of seismically active faults, the large earthquake corresponds to the collapse of the system, and the smaller earthquakes produce the perturbation of the system and at the same time reflect the increase of the response to the perturbation.

Intermediate-term earthquake prediction

- The high statistical significance of this kind of prediction was established on the basis of prediction of strong earthquakes in numerous regions world-wide, 1985 - 2001.
- Prediction is reproducible; complete formal definition of the algorithms was published in advance.

Real-time monitoring of the seismic flow

Italy: real time earthquake prediction experiment started in July 2003 (*Peresan al., Earth Sci. Rev. 2005*).

Algorithms fully formalized and globally tested for intermediate-term middle-range earthquake prediction are:

- **CN algorithm** (***Gabrielov et al., 1986; Rotwain and Novikova, 1999***)
- **M8S algorithm** ***Keilis-Borok and Kossobokov, 1987; Kossobokov et al., 2002***)

Updated predictions are regularly posted at:

www.ictp.trieste.it/www_users/sand/prediction/prediction.htm

Current predictions are accessible via password only, to prevent improper use of research on earthquake prediction but to permit rigorous *real time* test of the used methodologies

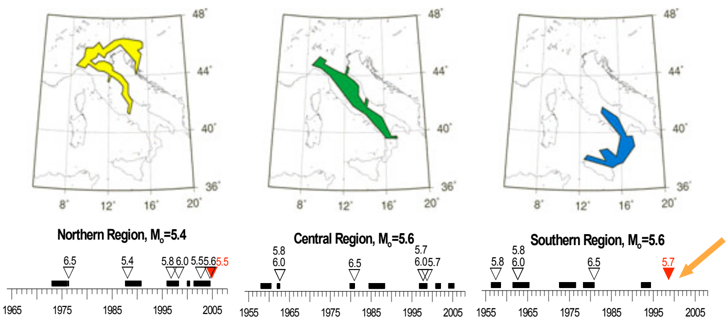

CN algorithm

Times of Increased Probability for the occurrence of events with M>Mo within the monitored regions

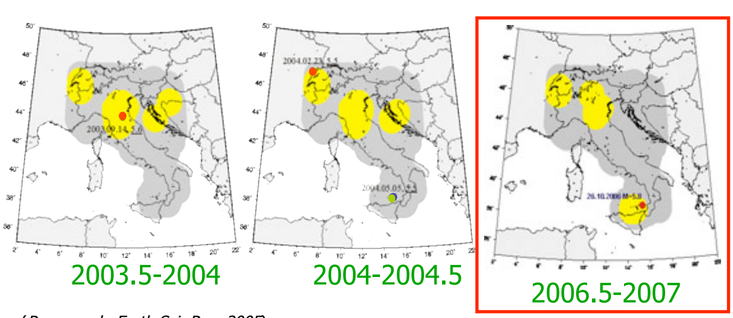

M8S algorithm

Monitored region

Alerted region

Events with M_{max} ≥5.5 occurred since July 2003

Updated to January 1 2009

(*Peresan al., Earth Sci. Rev. 2005*)

Space-time volume of alarm in M8S application in Italy

Experiment	M6.5+		M6.0+		M5.5+	
	Space-time volume, %	n/N	Space-time volume, %	n/N	Space-time volume, %	n/N
Retrospective (1972-2001)	36	2/2	40	1/2	39	9/14
Forward (2002-2008)	49	0/0	43	0/0	21	5/9
All together (1972-2008)	37	2/2	40	1/2	36	14/23

Algorithm M8s predicted 63% of the events occurred in the monitored zones in Italy, i.e. 17 out of 27 events occurred within the area alerted for the corresponding magnitude range. The confidence level of M5.5+ predictions since 1972 has been estimated to be above 98%; no estimation is yet possible for other magnitude levels.
(updated to January 1 2009)

http://www.ictp.trieste.it/www_users/sand/prediction/prediction.htm
http://www.mitp.ru/prediction.htm

Space-time volume of alarm in CN application in Italy

Experiment	Space-time volume of alarm (%)	n/N	Confidence level (%)
Retrospective* (1954 – 1963)	41	3/3	93
Retrospective (1964 – 1997)	27	5/5	>99
Forward (1998 – 2008)	29	4/5	97
All together (1954 – 2008)	30	12/13	99

* Central and Southern regions only

Algorithm CN predicted 12 out of the 13 strong earthquakes occurred in the monitored zones of Italy, with 30% of the considered space-time volume occupied by alarms.
(updated to January 1 2009)

http://www.ictp.trieste.it/www_users/sand/prediction/prediction.htm

Intermediate-term Intermediate-range earthquake prediction and Earth Observations

Integration with geodetic observations

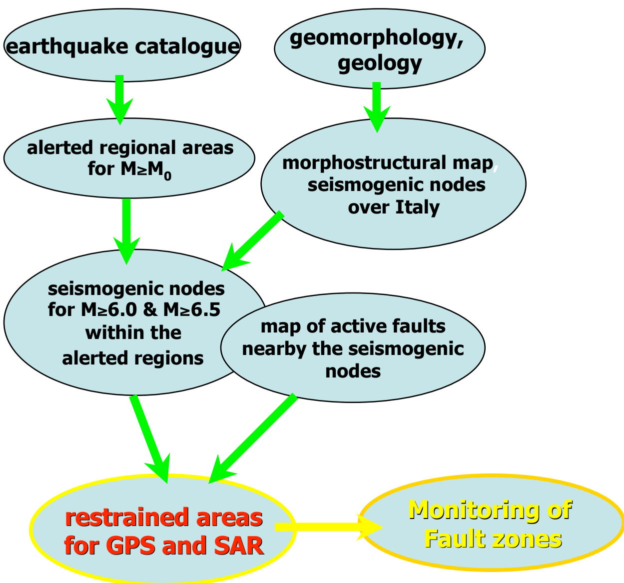

ASI Pilot Project - SISMA
"Seismic Information System for Monitoring and Alert"

Development of a system, based on the neo-deterministic approach for the estimation of seismic ground motion, integrating the space and time dependent information provided by real-time monitoring of seismic flow and EO data analysis, through geophysical forward modeling.

SISMA Overall Description

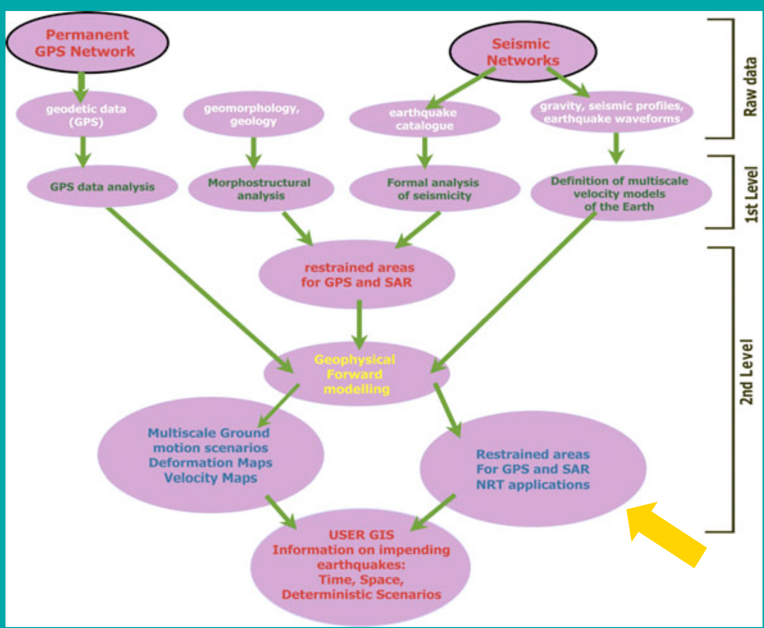

References

Ampferer, O., 1906. Uber das Bewegungbild von Faltengebirge, Austria. Geol. Bundesanst. Jahrb., 56, 539-622.
Chiarabba, C., et al., 2008. The southern Tyrrhenian subduction zone: Deep geometry, magmatism and Plio-Pleistocene evolution. Earth and Planetary Science Letters, 268, 408-423.
Baccheschi, P., Margheriti, L. and Steckler, M. S. (2007). Seismic anisotropy reveals focused mantle flow around the Calabrian slab (Southern Italy), G.R.L., 34, L05302, doi:10.1029/2006GL028899
Chimera, G., Aoudia, A., Saraoɪ, A. and Panza, G.F., (2003). Active tectonics in Central Italy: constraints from surface wave tomography and source moment tensor inversion. PEPI, 138, 241- 262.
Doglioni C., Green D. and Mongelli F. (2005): On the shallow origin of hotspots and the westward drift of the lithosphere: in Plates, Plumes and Paradigms, G.R. Foulger, J.H. Natland, D.C. Presnall, & D.L. Anderson (Eds), GSA Sp. Paper 388, 735-749.
Doglioni C., Carminati E., Cuffaro M. and Scrocca D. (2007): Subduction kinematics and dynamic constraints. Earth Science Reviews, 83, 125-175, doi:10.1016/j.earscirev.2007.04.001.
Ismail-Zadeh, A.T., Aoudia, A., and Panza, G.F., (2004). Tectonic Stress in the Central Apennines due to Lithospheric Buoyancy. Doklady Earth Sciences, 395A, 3, 2004, 369-372.
Ismail-Zadeh, A.T., Aoudia, A., and Panza, G.F., (2009). Three-dimensional numerical modeling of contemporary mantle flow and tectonic stress beneath the Central Mediterranean, submiited.
Kelly, R.K., Kelemen, P.B., Jull, M., 2003. Buoyancy of the continental upper mantle. G3. 4 (2), 1017.
Mueller, S. and Panza, G.F., (1986). Evidence of a deep-reaching lithospheric root under the Alpine Arc. In: The Origin of Arcs, ed. by: F.C. Wezel, Elsevier, 21, 93-113.
Panza, G.F., Mueller, S., 1978. The plate boundary between Eurasia and Africa in the Alpine Area. Mem. Soc. Geol. It., 33, 43-50.
Panza, G.F., Calcagnile, G., Scandone, P. and Mueller, S., (1980). La struttura profonda dell' Area Mediterranea. Le Scienze, 141, 60-69.
Panza, G.F., Mueller, S., Calcagnile, G. and Knopoff, L., (1982). Delineation of the north central Italian upper mantle anomaly. Nature, 296, 238-239.
Panza, G. F., Raykova, R. B., Carminati, E., Doglioni, C., (2007). Upper mantle flow in the western Mediterranean. EPSL, 257, 200-214.
Peccerillo, A., 2005. Plio-Quaternary volcanism in Italy. Springer, Heidelberg, 365 pp.
Raykova, R.B. and Panza, G.F., (2006). Surface waves tomography and non-linear inversion in the southeast Carpathians. Physics of the Earth and Planetary Interiors, 157, 164-180

References

Scalera, G., 2007. A new model of orogenic evolution Rend. Soc. Geol. It., 5, Nuova Serie, 214-218.
Scalera, G., 2005. A new interpretation of the Mediterranean arcs: Mantle wedge intrusion instead of subduction Boll. Soc. Geol.It., Volume Speciale n. 5, 129-147.
Scalera, G., 2008 Great and old earthquakes against great and old paradigms – paradoxes, historical roots, alternative answers. Adv. Geosci., 14, 41–57, 2008
Scoppola B., Boccaletti D., Bevis M., Carminati E. and Doglioni C. (2006): The westward drift of the lithosphere: a rotational drag? Bull. Geol. Soc. Am., 118, 1/2; p. 199–209; doi: 10.1130/B25734.1.
Spakman, W., Wortel, M. J. R., Vlaar, N. J. (1988):. The Hellenic subduction zone: A tomographic image and its geodynamic implications, G.R.L., 15, 60-63.
Zhang, Yu-Sh. and Tanimoto, T. (1992) Ridges, hotspots and their interaction as observed in seismic velocity maps. Nature, 355, 45 - 49; doi:10.1038/355045a0.